

1 **Multi-Satellite Retrieval of SSA using OMI-MODIS algorithm**

2 Kruthika Eswaran<sup>1,2\*</sup>, Sreedharan Krishnakumari Satheesh<sup>1,2</sup> and Jayaraman Srinivasan<sup>1,2</sup>

3 <sup>1</sup> Centre for Atmospheric and Oceanic Sciences, Indian Institute of Science, Bangalore, India

4 <sup>2</sup> Divecha Centre for Climate Change, Indian Institute of Science, Bangalore, India

5 *\*Correspondence to:* Kruthika Eswaran (kruthika.eswaran89@gmail.com)

6 **Abstract** - Single scattering albedo (SSA) represents a unique identification of aerosol type and  
7 can be a determinant factor in the estimation of aerosol radiative forcing. However, SSA  
8 retrievals are highly uncertain due to cloud contamination and aerosol composition. The recent  
9 improvement in the SSA retrieval algorithm has combined the superior cloud-masking technique  
10 of the Moderate Resolution Imaging Spectroradiometer (MODIS) and the better sensitivity of the  
11 Ozone Monitoring Instrument (OMI) to aerosol absorption. The combined OMI-MODIS  
12 algorithm has been validated over a small spatial and temporal scale only. The present study  
13 validates the algorithm over global oceans for the period 2008-2012. The geographical  
14 heterogeneity in the aerosol type and concentration over the Atlantic Ocean, the Arabian Sea and  
15 the Bay of Bengal was useful to delineate the effect of aerosol type on the retrieval algorithm.  
16 We also noted that OMI overestimated SSA when absorbing aerosols were present closer to the  
17 surface. We attribute this overestimation to data discontinuity in the aerosol height climatology  
18 derived from Cloud-Aerosol Lidar and Infrared Pathfinder Satellite Observations (CALIPSO)  
19 satellite. OMI uses pre-defined aerosol heights over regions where CALIPSO climatology is not  
20 present leading to overestimation of SSA. The importance of aerosol height was also studied  
21 using the Santa Barbara DISORT radiative transfer (SBDART) model. The results from the joint  
22 retrieval were validated with cruise-based measurements. It was seen that OMI-MODIS SSA  
23 retrievals performed better than OMI only retrieval over the Bay of Bengal during winter when

24 the aerosols are present closer to the surface. Discrepancy between satellite retrievals and cruise  
25 measurements was seen when elevated aerosols are present which might not be detected by the  
26 cruise instruments.

## 27 **1. Introduction**

28 Aerosols of different types are spatially distributed heterogeneously and at different altitudes in  
29 the atmosphere. Depending upon their properties, certain aerosols types such as carbonaceous  
30 aerosols emitted from biomass burning warm the atmosphere by absorbing radiation, while other  
31 aerosol types such as sea salt emitted from the oceans cool the atmosphere by scattering radiation  
32 (Ramanathan et al., 2001). Due to the opposing effects on the atmosphere aerosols can have  
33 either net warming or cooling effect on the global climate depending upon the aerosol type,  
34 concentration and vertical distribution. Effect of natural and anthropogenic aerosols on the global  
35 climate is measured by 'aerosol radiative forcing' (the perturbation to the earth's radiation budget  
36 caused by the presence of aerosols). Positive forcing implies atmospheric warming and vice-  
37 versa. (Liao and Seinfeld, 1998; Podgorny and Ramanathan, 2001; Satheesh, 2002; Johnson et  
38 al., 2003; Kim et al., 2004; Moorthy et al., 2004; Meloni et al., 2005; Satheesh and Moorthy,  
39 2005; Seinfeld and Pandis, 2006; Satheesh et al., 2008; Chand et al., 2009; Mishra et al., 2015).  
40 According to the climate assessment report, the estimation of aerosol radiative forcing (due to  
41 anthropogenic aerosols) is a major cause of uncertainty in the estimation of climate sensitivity  
42 and therefore presents a significant impediment to climate modelling (IPCC, 2013). The  
43 uncertainty is mostly due to the lack of accurate measurement of the scattering and absorbing  
44 properties of the aerosols (Cooke and Wilson, 1996; Menon et al., 2002; Chung and Seinfeld,  
45 2002; Bond and Sun, 2005).

46 The Single Scattering Albedo (SSA), (the fraction of the total extinction of radiation

47 attributed to scattering) is used to distinguish the scattering and absorbing properties of aerosols.  
48 SSA represents a unique fingerprint of the type of aerosol and its radiative forcing (Hansen et al.,  
49 1997; Haywood et al., 1997; Myhre et al., 1998). In general, purely scattering aerosols have SSA  
50 value of approximately 1 while highly absorbing aerosols have SSA less than 0.7. However,  
51 SSA retrievals lack high certainty (Bond and Bergstrom, 2006; Bond et al., 2013). Uncertainties  
52 in SSA retrievals are due to factors such as cloud contamination, instrumentation error and  
53 aerosol modification due to atmospheric processes. A small change in SSA can cause the aerosol  
54 radiative forcing to change from negative to positive (Hansen et al., 1997; Seinfeld and Pandis,  
55 2006). Loeb and Su (2010) performed a radiative perturbation analysis and found that direct  
56 aerosol radiative forcing was highly sensitive to small perturbations in SSA under clear-sky and  
57 cloudy-sky conditions. A simulation study using Santa Barbara DISORT Radiative Transfer  
58 (SBDART) model in the present work (Section 5.3) shows that a change in SSA from 0.8 to 1  
59 can induce a change of  $4 \text{ Wm}^{-2}$  in the top-of-atmosphere (TOA) flux depending on the aerosol  
60 type and aerosol layer height (Figure 8). Better SSA retrievals (both in-situ and satellite-based)  
61 are required to reduce the uncertainty in SSA for a more accurate estimation of aerosol forcing;  
62 particularly over regions influenced by a variety of air masses. There is also a need for accurate  
63 spectral aerosol absorption measurements, which is required to validate SSA derived from  
64 satellites (Bergstrom et al., 2007).

65 Studies on the various measurements of aerosol light absorption using instruments and their  
66 uncertainty evaluation have been performed previously (Horvath, 1993, Heintzenberg et al.,  
67 1997; Moosmuller et al., 2009). The different methods of retrieval of SSA, both ground-based  
68 and using satellites, are provided in Table 1. Unlike aerosol absorption coefficient, SSA is not  
69 measured directly by an instrument. Instead, it is retrieved using lookup tables or estimated using

70 other parameters which are measured or calculated using models.

71        Though these previous studies on ground-based retrievals have brought a fundamental  
72 understanding of the estimation of amounts of aerosols / aerosol chemistry, their restricted spatial  
73 and temporal extent is a significant limitation. Moreover, these studies have reduced availability  
74 of scenes for indirect retrievals. Some techniques are limited due to cloud contamination while  
75 others operate only under specific conditions (e.g. presence of sun glint). This presents a need for  
76 better SSA retrieval algorithms that overcome the present technical limitations, and that can be  
77 applied on a global scale. The global extent of observations from satellites has increased the  
78 spatial extent of the observations (Kaufman et al., 2002a). Though the satellite-based SSA  
79 retrievals have been shown to be extremely successful over the majority of ocean and land  
80 regions, they still have a limited success over deserts and ice sheets. Over deserts and ice-sheets,  
81 high surface reflectance affects the satellite retrievals in the visible spectrum. To counter this,  
82 SSA is retrieved in the UV spectrum (330 nm to 400 nm) over these regions (Torres et al., 1998,  
83 2007). In the UV spectrum, the upwelling radiances are highly sensitive to the aerosol absorption  
84 and also have a lower influence of surface albedo (Torres et al., 2007). SSA retrieval in UV  
85 spectrum hence avoids difficulties encountered over surfaces with high albedo.

86        The quality of OMI SSA retrievals is affected by sub-pixel cloud contamination (due to the  
87 larger footprint of size 13km x 24km) and uncertainty in the assumption of spectral surface  
88 albedo (Torres et al., 2007). To counter the problems and uncertainties in the OMI SSA retrieval  
89 (Table 2), Satheesh et al. 2009 used retrievals from multiple satellites. They used combined  
90 retrievals from OMI-MODIS since each of these sensors have their own strengths and both fly  
91 within ~7-8 minutes of each other in the A-train constellation (Stephens et al., 2002). The better  
92 cloud-screened retrieval of AOD from MODIS (Levy et al., 2003; 2013) and the high sensitivity

93 of OMI to aerosol absorption was used to develop a hybrid algorithm to retrieve SSA (Satheesh  
94 et al., 2009). The algorithm uses the MODIS AOD as a reference to infer the aerosol layer height  
95 and SSA from OMI. This removes any *a priori* assumption made by the OMI algorithm to  
96 retrieve ALH along with SSA. The study by Satheesh et al. 2009 was performed over the East  
97 tropical Atlantic Ocean, the Central tropical Atlantic Ocean and the Arabian Sea for the year  
98 2006. A comparison of the retrieved aerosol height with aircraft measurements showed that OMI-  
99 MODIS was more accurate than OMI. Gassó and Torres (2016) performed a detailed analysis of  
100 the OMI UV product retrievals over oceans and island sites. They compared the OMI retrieved  
101 AOD with MODIS and AERONET (Aerosol Robotic Network) AODs. They also used the OMI-  
102 MODIS algorithm for only two particular cases over and near Africa to understand how the  
103 assumption of aerosol height and shape affected AOD and SSA retrievals. When the actual height  
104 from satellite Lidar was used instead of climatological values, and when the shape of dust  
105 aerosols was assumed to be non-spherical, the retrievals by OMI agreed better with other  
106 observations including the original OMI-MODIS method. The OMI-MODIS algorithm has been  
107 used in calculating aerosol radiative forcing (Satheesh et al., 2010) over oceanic regions  
108 surrounding India and used in retrieving SSA over land (Narasimhan and Satheesh, 2013) as well  
109 as used to understand the retrievals of OMI UV products for two particular cases (Gassó and  
110 Torres, 2016). However, a detailed analysis of the algorithm on a larger spatial and temporal  
111 scale has not been done so far.

112 The current work applies the OMI-MODIS algorithm to retrieve SSA on a global scale. It is  
113 applied over the global oceans from 2008-2012. Regional analysis over the Atlantic, the Arabian  
114 Sea and the Bay of Bengal are done by incorporating the aerosol layer height and the type of  
115 aerosols. After estimating SSA values using the OMI-MODIS algorithm, the present study then

116 uses cruise measurements of SSA from the Integrated Campaign for Aerosols, Gases and  
117 Radiation Budget (ICARB) and winter ICARB campaigns over Arabian Sea and Bay of Bengal  
118 in 2006 and 2009 to validate the same (Moorthy et al., 2008, 2010).

## 119 **2. Data**

### 120 **2.1. OMI**

121 The Ozone Monitoring Instrument (OMI) onboard the Aura satellite was launched in 2004. For  
122 OMI measurements two aerosol inversion schemes are used- OMI near UV (OMAERUV)  
123 algorithm and the multi-wavelength (OMAERO) algorithm (Torres et al., 2007). The OMAERO  
124 algorithm uses 19 wavelengths in the range of 330-500 nm to retrieve corresponding aerosol  
125 characteristics. For the present study, we have used the OMAERUV algorithm which uses  
126 measurements at two wavelengths 354 nm and 388 nm. The reason behind choosing these  
127 wavelengths is the high sensitivity of upwelling radiances to aerosol absorption and the lower  
128 influence of surface in measurements due to low reflectance values in the UV region. In addition  
129 to this, the wavelengths also have negligible interference from trace gases. This gives a unique  
130 advantage of retrieving aerosol properties over ocean and land including arid and semi-arid  
131 regions (Torres et al., 1998; 2007).

132 The products derived from the algorithm include AOD, absorption aerosol optical depth  
133 (AAOD) and single scattering albedo (SSA). These are derived from pre-computed reflectance  
134 values for different aerosol models. Three major types of aerosols have been used - Desert dust,  
135 carbonaceous aerosols from biomass burning and background and urban-industrial aerosols.  
136 Each type has seven models of SSA. The retrieved products of OMAERUV are sensitive to the  
137 aerosol layer height (Torres et al., 1998) and are reported for five discrete aerosol layer heights,  
138 i.e., surface (exponential profile), 1.5, 3.0, 6.0, and 10.0 km with latter four following a Gaussian

139 distribution.

140 Due to the high sensitivity of SSA retrieval to the assumption of aerosol height and aerosol  
141 type (Torres et al., 2002), the OMI algorithm was improved (Collection 003-PGE V1.4.2, Torres  
142 et al., 2013). The climatology of aerosol layer height from CALIPSO (Cloud-Aerosol Lidar and  
143 Infrared Pathfinder Satellite Observations) along with carbon monoxide (CO) measurements  
144 from AIRS (Atmospheric Infrared Sounder) have helped distinguish carbonaceous aerosols from  
145 dust particles. Torres et al. (2013) showed that the combined use of AIRS CO measurements and  
146 OMI Aerosol Index (AI) retrievals, helped in identifying the type of absorbing aerosol. Thus,  
147 smoke layers were identified when values of AI and CO measurements were high, and during  
148 events of high AI and low CO values, the aerosols were identified as dust. The AIRS CO  
149 measurements were also used to identify large aerosol loading which was otherwise represented  
150 as clouds by the OMAERUV algorithm. Using collocated observations of OMI and Cloud-  
151 Aerosol Lidar with Orthogonal Polarization (CALIOP), Torres et al. (2013) estimated the height  
152 of elevated absorbing aerosols for a 30-month period from July 2006 to December 2008. An  
153 effective aerosol layer height was calculated using the CALIOP 1064 nm attenuated backscatter  
154 weighted by corresponding altitudes. The 30-month climatology of aerosol height was used in  
155 the OMAERUV retrievals which then validated against the AERONET observations (Torres et  
156 al., 2013). The results showed that there was an improvement in the retrievals.

157 Since 2007, observations have been affected by an instrumental issue called the *row*  
158 *anomaly* which reduces the quality of radiance at all wavelengths (Jethva et al., 2014). Torres et  
159 al. (2018) studied the impact of row anomaly on the OMAERUV retrievals by comparing  
160 monthly values AOD, SSA and UV aerosol index (UVAI) of two different sets of scattering  
161 angles. Over regions dominated by carbonaceous and sulphate aerosols, the agreement between

162 the sets was better than over arid regions dominated by dust aerosols. Differences were also  
163 found over cloudy regions. The discrepancies were attributed to the inaccurate representation of  
164 scattering effects of dust aerosols and cloud droplets. Better representation of scattering by  
165 clouds and the non-spherical (spheroidal) shape assumption of dust aerosols was found to reduce  
166 the inconsistencies in aerosol products due to row anomaly. These improvements have been  
167 incorporated in the latest version of OMAERUV product (version 1.8.9) which has been used in  
168 the present study. Along with the aerosol products retrieved at different heights, the final set of  
169 AOD/SSA/AAOD retrievals in the OMAERUV product is reported at the mean ALH provided  
170 by the 30-month long averaged climatology developed using OMI-CALIOP combined  
171 observations (Torres et al., 2013). The original aerosol height assumptions were used in the  
172 algorithm over regions where the climatology was unavailable.

## 173 **2.2. MODIS**

174 The Moderate Resolution Imaging Spectrometer (MODIS) instrument on the Aqua satellite  
175 was launched in 2002. This instrument, with 36 spectral channels has a unique ability to retrieve  
176 aerosol properties with better accuracy over both land and ocean (Remer et al., 2005; Levy et al.,  
177 2003). Of these, seven channels (0.47-2.13  $\mu\text{m}$ ) are used to retrieve aerosol properties over the  
178 ocean (Tanré et al., 1997).

179 As described in Remer et al., (2005), before the retrieval algorithm, masking of sediments,  
180 clouds and ocean glint is performed to separate valid pixels from bad ones. The retrieval  
181 algorithm of MODIS (also called the inversion procedure) has been described in detail  
182 previously (Tanré et al., 1997; Levy et al., 2003; Remer et al., 2005). The algorithm uses a ‘look-  
183 up table’ (LUT) approach, i.e., for a set of aerosol and surface parameters, radiative transfer  
184 calculations are performed. Spectral reflectance derived from the LUT is compared with



185 MODIS-measured spectral reflectance to find the ‘best’ (least-squares) fit. The resulting  
186 combination of modes provides the aerosol model from which size distribution, properties  
187 including spectral optical depth, effective radius are derived. The product used from MODIS is  
188 the Level 2 aerosol (MYD04, Collection 5.1) product. The parameter chosen is  
189 'Effective\_Optical\_Depth\_Average\_Ocean' which provides the aerosol optical depth over the  
190 ocean at seven wavelengths. The value is the average of all the solutions in the inversion  
191 procedure with the least-square error < 3%.

192 A combination of OMI and MODIS helps indirectly in counteracting the cloud  
193 contamination problem and also uses the strength of the individual sensors – OMI's sensitivity to  
194 aerosol absorption combined with the better cloud screening of MODIS and accurate retrieval of  
195 AOD, and aerosol size (Satheesh et al., 2009; Narasimhan and Satheesh, 2013).

### 196 **3. Algorithm**

197 MODIS aerosol product reports retrievals at 10 x 10 km spatial resolution at nadir (and a cloud  
198 mask at 500m and 1km resolution) whereas OMI reports at 13 km x 24 km. This results in an  
199 OMI pixel being prone to cloud contamination which may result in an overestimation in AOD  
200 and SSA (Torres et al., 1998). However, AAOD can be retrieved in the presence of small cloud  
201 contamination since there is cancellation of errors (Torres et al., 2007).

202 The high accuracy of size-resolved aerosol retrievals with MODIS is because the over-ocean  
203 algorithm employs all seven channels (0.47-2.13 micron) in the inversion enabling better  
204 characterization of fine and coarse particles. (Tanré et al., 1997; Remer et al., 2005; Levy et al.,  
205 2003). While OMI is highly sensitive to aerosol absorption in the near-UV region, the accuracy  
206 in the retrieval of AAOD depends on the aerosol layer height assumption. OMI provides AOD  
207 and AAOD at different heights as prescribed by various aerosol types (Torres et al., 2007).

208 The assumption of aerosol layer height in the OMI algorithm constraints the retrievals of  
209 AOD and SSA. The approach proposed in Satheesh et al. (2009) used MODIS AOD as an input  
210 to the OMI retrieval algorithm so that the MODIS AOD constraints the OMI inversion so that the  
211 OMI inversion is free to infer the aerosol layer height and SSA. Satheesh et al. (2009)  
212 extrapolated MODIS AOD from the visible to 388nm and compared the estimated UV AOD with  
213 high quality ground-based AERONET observations. The deviation between linearly-extrapolated  
214 MODIS AOD and AERONET AOD was more significant at higher AERONET AOD values.  
215 This was attributed to the presence of a large number of fine-mode aerosols which caused a  
216 nonlinear curvature to the AOD spectral dependence and affected AOD at UV wavelengths.  
217 Hence to improve the linear extrapolation, information on the aerosol spectral curvature was also  
218 included. This was achieved by using an average regression equation to correct the MODIS AOD  
219 (Satheesh et al., 2009; Equation 3). They showed that MODIS AOD could be first linearly  
220 extrapolated to 388 nm and then corrected for curvature before being used as input to the OMI  
221 retrieval algorithm. The present work uses the same algorithm as proposed by Satheesh et al.  
222 (2009) to retrieve SSA over the oceans for the region 60S-60N and 180W-180E from December  
223 2007-November 2012. The methodology is described in detail in the following section.

#### 224 **4. Methodology**

225 The AOD for ocean obtained from the Level 2 aerosol product of Aqua-MODIS (MYD04) was  
226 used. Using linear extrapolation with spectral curvature correction (Satheesh et al., 2009), AOD  
227 at 388 nm (hereafter,  $AOD_{388}$ ) was calculated from AOD at seven wavelengths ranging from  
228 0.47-2.13  $\mu\text{m}$ . OMI provides AOD and SSA for five different aerosol layer heights starting from  
229 the surface and at 1.5, 3.0, 6.0 and 10.0km ( $AOD_{\text{OMI}}$  and  $SSA_{388}$ ). It also provides the best  
230 estimate of SSA calculated based on the CALIOP aerosol layer height climatology ( $SSA_{\text{OMI}}$ ).

231 For the present study, polar regions are not included. Hence pixels from both OMI and  
232 MODIS that are outside the 60S-60N and 180W-180E region are excluded. Pixels with invalid or  
233 missing values are also excluded. The various parameters extracted from the data were re-  
234 gridded onto a uniform grid of  $0.5^\circ \times 0.5^\circ$  within the region of study to reduce computation time.  
235 For both the satellites, this procedure was repeated for each swath data which were then  
236 combined to calculate the daily means.

237 The daily data from collocated MODIS and OMI were utilised in the final algorithm. As  
238 mentioned before OMI provides AOD and SSA for five different aerosol layer heights. Using  
239  $AOD_{388}$  as the reference, the corresponding aerosol layer height was calculated from the five  
240  $AOD_{OMI}$  values through linear interpolation. This height is then used as a reference to find the  
241 SSA using interpolation from the set of  $SSA_{388}$  values. Finally, this SSA ( $SSA_{OMI-MODIS}$ ), and the  
242 best estimate of SSA ( $SSA_{OMI}$ ) were compared with each other.

## 243 **5. Results**

244 The spatial distribution of SSA retrieved using OMI is shown in Fig. 1a. The values are averaged  
245 over five years and plotted seasonally.

246 The SSA retrieved using OMI-MODIS algorithm is shown in Fig. 1b.

247 SSA over open oceans is close to 1 due to the presence of a large amount of sea-salt and  
248 sulphate. Closer to land, a variety of aerosols are present which results in SSA varying from 0.85  
249 to  $\sim 1$ . Over the oceans, separation of ocean colour effects and aerosol concentrations is difficult.  
250 Hence the OMI algorithm retrieves when enough absorbing aerosols are present, i.e.  $AI \geq 0.8$   
251 (Torres et al., 2013). Only pixels whose quality has been assigned as 0 or the highest quality by  
252 OMI have been used. The points flagged for row anomaly are also not used in this study. Thus,  
253 the retrievals did not cover the entire globe. From Fig.1a it can be seen that majority of the valid

254 SSA retrievals were over major aerosol sources in the world and not over remote oceanic regions  
255 like central equatorial Pacific or Antarctic ocean. The major sources include the vast biomass  
256 outflow over the Atlantic Ocean from the west coast of Africa, the dust over the Arabian Sea  
257 from the arid areas of Arabia & Africa and the dust blown over the Atlantic Ocean from the  
258 Sahara. Other regions like the east coast of China, the Bay of Bengal are influenced by a variety  
259 of anthropogenic aerosols during different seasons. In the OMI-MODIS algorithm, the aerosol  
260 layer height is retrieved through linear interpolation of  $AOD_{OMI}$  at five different heights and  
261  $AOD_{388}$  as a reference. Linear interpolation was not performed for OMI retrievals which had a  
262 missing value at any particular height or if the OMI retrieval was the same at all heights. Such  
263 OMI-MODIS values were considered to be invalid. Similarly, if the MODIS AOD was found to  
264 be missing or invalid, the corresponding OMI-MODIS retrieval was also considered invalid. This  
265 resulted in a reduction in the total number of valid points in OMI-MODIS algorithm when  
266 compared to OMI algorithm (Fig. 1b). However, both the algorithms capture the major oceanic  
267 regions which are influenced by a large number of aerosols. Gassó and Torres (2016) for a  
268 particular day over the North Central Atlantic compared the AOD values retrieved by OMI and  
269 MODIS. They compared the difference with the aerosol cloud mask retrieved by MODIS. It was  
270 found that while most of the retrievals of OMI screened the cloudy pixels, some of the best  
271 quality (flag=0) pixels were found to be cloud contaminated. They attributed the contamination  
272 to the coarser pixel size of OMI compared to the smaller pixel size of MODIS cloud product. At  
273 higher cloud fraction, OMI retrieved values implying that they can detect aerosol above clouds  
274 or the pixels are prone to cloud contamination. Gassó and Torres concluded that only MODIS  
275 cloud fraction could not be used to screen out OMI pixels. A larger spatiotemporal scale of such  
276 an analysis is required but is beyond the scope of this manuscript and will be addressed in the

277 future. However, OMI retrievals at higher cloud fraction could be the reason for more points in  
278 Fig. 1a than OMI MODIS in Fig. 1b.

279 Two important regions over oceans influenced by a variety of aerosols are the tropical  
280 Atlantic Ocean and the oceans around the Indian subcontinent. The new approach was used over  
281 these regions- Atlantic (5N-30N; 60W-20W) (ATL) and Arabian Sea and Bay of Bengal (0-25N;  
282 55E-100E) (ARBOB).

### 283 **5.1. Difference in SSA retrieval algorithms during different seasons**

284 To understand how the OMI-MODIS algorithm compares with the retrieval using the existing  
285 OMI algorithm, the difference between  $SSA_{\text{OMI-MODIS}}$  and  $SSA_{\text{OMI}}$  ( $\Delta SSA$ ) averaged over five  
286 years for different seasons is shown in Fig. 2.

287 During March-April May (MAM) and June-July-August (JJA), there is a longitudinal  
288 gradient in  $\Delta SSA$  from the coast of Sahara towards the open Atlantic Ocean. Kaufman et al.  
289 (2002a) showed that close to the coast of Africa, aerosols are more absorbing than those away  
290 from the coast. The difference in the type of aerosols as we move away from the coast could be  
291 one of the reasons for the gradient in  $\Delta SSA$ . The difference can also be attributed to the shape of  
292 dust aerosols which are present in large numbers near the coast of Africa (Torres et al., 2018).  
293 The  $\Delta SSA$  changes sign with season. This was attributed to the change in aerosol layer height  
294 and (or) aerosol physical and optical properties.

295 Both ATL and ARBOB regions are influenced by the type of aerosols which result in a  
296 complex mixture and eventually resulting in the variation in SSA distribution over each season.  
297 While the spatial plot of  $\Delta SSA$  in Fig. 2 represents the regions where maximum and minimum  
298 differences are located around the globe, a distribution plot provides the ranges of  $\Delta SSA$  which  
299 dominate and which do not. The distribution of  $\Delta SSA$  for different seasons averaged over five

300 years (2008-2012) is plotted in Fig. 3a and 3b for the regions- ATL and ARBOB respectively.

301 Over the tropical Atlantic Ocean,  $\Delta$ SSA was found within  $\pm 0.03$  >80% of the time during  
302 all the seasons. Over Arabian Sea and Bay of Bengal, the values of SSA matched within  $\pm 0.03$   
303 during MAM when dust is present in large quantity over the region. However,  $\Delta$ SSA has values  
304 lower than  $< -0.03$  especially during the seasons of JJA and SON. Satheesh et al. (2009) showed  
305 in their analysis that the reason for the discrepancies during non-dust seasons could be due to the  
306 wrong assumption of aerosol layer height (ALH) or due to the wrong assumption of aerosol  
307 model. Before understanding the role of ALH in SSA retrieval, the meteorological conditions of  
308 the ARBOB region (Arabian Sea and Bay of Bengal separately), for different seasons are studied  
309 and trajectory analysis is done. This helps in identifying major sources of aerosols during each  
310 season.

## 311 **5.2. Trajectory analysis**

### 312 **Arabian Sea and Bay of Bengal (ARBOB)**

313 The Arabian Sea and the Bay of Bengal are oceanic regions on the west and east coast of  
314 India respectively. Both regions are influenced by various types of aerosols during different  
315 seasons. The Arabian Sea has been dominated by dust aerosols and is influenced by high levels  
316 of dust during certain seasons as seen from satellite images (Sirocko and Sarnthein, 1989). Pease  
317 et al. (1998) studied the geochemistry and the transport of various dust samples during different  
318 cruises in different seasons. During winter and summer, the pattern of aerosol transport was  
319 similar to that of the Indian monsoon pattern – northeasterly (winter) and southwesterly  
320 (summer). Thus, the major sources of aerosols were the Arabian Peninsula (including Saharan  
321 dust and the Middle East) and Indian sub-continent in summer and winter respectively. The mean  
322 7-day back trajectory using HYSPLIT model from a point over the Arabian Sea (15N; 65E) was

323 performed for each season of 2010 and at three different heights (500m, 1500m and 2500m  
324 above MSL). The Arabian Sea region was divided into four quadrants – 1) Arabian Peninsula and  
325 North Africa, 2) Central Africa, 3) Indian sub-continent and 4) Indian Ocean and Southeast Asia  
326 (Fig. 4). The influence of different aerosol source regions over the Arabian Sea is given in Table  
327 2.

328 Similar to Pease et al. (1998), Tindale and Pease (1999) found that transport of aerosols near  
329 the surface followed the surface wind currents. The dust content was low near the surface during  
330 summer due to the presence of Findlater jet, but the general dust concentrations were higher than  
331 other oceanic regions. During winter, the winds are predominantly north and northeasterly and  
332 hence results in transport of aerosols from India/Pakistan/Afghanistan onto the Arabian Sea.  
333 However, the presence of anticyclonic circulation over Arabia (20N; 60E) results in  
334 northwesterly winds transporting dust over the Arabian Sea (Rajeev et al., 2000). The springtime  
335 (March-April-May) is the transition between northeast and southwest monsoon. The winds  
336 become south westerlies which result in the advection of aerosols from the open Indian Ocean or  
337 near Somalia. At higher altitudes (above the Findlater jet) dust transport occurs from Arabia.  
338 During summer, the southwest monsoon wind patterns carry aerosols from southeast/east Indian  
339 Ocean (mainly sea-salt). As the altitude increases, the wind patterns change a little due to  
340 aerosols coming from southwest Indian Ocean/Somalia. Above the Findlater jet, as explained by  
341 Tindale and Pease (1999), dust transport occurs from Arabian Peninsula (Table 2).

342 Being an integral part of the Indian Summer Monsoon, studies over the Bay of Bengal is  
343 important especially the role of aerosols in the local climate change. While the Arabian Sea is  
344 dominated by dust and oceanic aerosols, studies have shown that the Bay of Bengal is influenced  
345 by various air masses associated with Asian monsoon system including those of anthropogenic

346 origin (Krishnamurti et al., 1998). The synoptic meteorological conditions over the Bay of  
347 Bengal have been studied in detail by Moorthy et al. (2003) and Satheesh et al. (2006). Similar to  
348 the other two regions, mean 7-day back trajectory analysis from a point over (15N; 90N) was  
349 performed for each season of 2010 and at three different heights (500m, 1500m and 2500m  
350 above MSL). The four quadrants representing the various aerosol source regions are 1)  
351 India/Arabian Peninsula, 2) Indian Ocean, 3) North/Northeast India and East Asia and 4)  
352 Southeast Asia (Fig. 5). Table 3 represents the influence of aerosol source regions over the Bay  
353 of Bengal.

354 The northwesterly winds occur from west to east in the Indo-Gangetic Plain (IGP), and due  
355 to subsidence, the aerosols are trapped in the east during winter (Dey and Di Girolamo, 2010; Di  
356 Girolamo et al., 2004). The IGP with its dense population and a large number of industries acts  
357 as a source for anthropogenic aerosols which are transported to Bay of Bengal during winter  
358 (Kumar et al., 2013). Along with mineral dust from the Arabian Peninsula, biomass aerosols  
359 from Southeast Asia are also transported to the bay. Field experiments like ICARB (Moorthy et  
360 al., 2008) during the springtime (pre-monsoon) showed transports of aerosols from the Arabian  
361 Peninsula and also the presence of elevated aerosols (anthropogenic and natural) over Bay of  
362 Bengal (Satheesh et al., 2008). The post-monsoon season acts as a transition from the summer to  
363 winter monsoon. The winds during September are still south westerlies and during October weak  
364 westerlies are present (Lawrence and Lelieveld, 2010). This results in transportation of aerosols  
365 from the Indian Ocean and the Arabian Sea. Thus, from Table 3 it can be seen that both  
366 anthropogenic aerosols (from IGP, Southeast Asia) and natural aerosols (marine and dust) are  
367 present over the Bay of Bengal during different seasons.

### 368 **5.3. Role of Aerosol Layer Height in SSA retrieval**



369 Sathesh et al. (2009) devised a new algorithm to improve the retrieval of SSA using  
370 combined OMI and MODIS data. They used MODIS-predicted UV AOD as the input to improve  
371 the original OMI algorithm, which was constrained by the assumption of aerosol layer height.  
372 Over the Atlantic, they found that on an average the AOD values retrieved from both algorithms  
373 agreed within  $\pm 0.1$ . However, over the Arabian Sea only when there was considerable loading of  
374 dust (especially during the March-April-May season), the OMI AOD and MODIS AOD had  
375 agreement suggesting that during other seasons, the assumption of aerosol height could be  
376 wrong. Sathesh et al. (2009) also found that over the Arabian Sea the aerosol layer height  
377 (ALH) derived from OMI-MODIS algorithm agreed well with aircraft measurements when  
378 compared to OMI SSA retrieval. In the current work, the aerosol layer height (ALH) provide by  
379 OMI, is the mean climatological height (section 2.1). For OMI-MODIS the ALH is estimated  
380 from OMI AOD values (at five different heights) by linear interpolation using  $AOD_{388}$  as a  
381 reference (section 4). The difference in aerosol layer height (ALH) between OMI-MODIS and  
382 OMI was plotted against the difference in SSA over the Arabian Sea and Bay of Bengal (Fig. 6a).  
383 The colorbar represents ALH estimated by OMI-MODIS algorithm. The most important  
384 observation from this analysis was that OMI overestimated SSA when it overestimated ALH  
385 (compared to OMI-MODIS) and vice versa. It has been shown by Gassó and Torres (2016) that  
386 when the actual aerosol height measured by Satellite Lidar was 1.5km more than the  
387 climatological or assumed height, OMI retrieved higher SSA. It can be seen from Fig. 6a, the  
388 blue coloured circles represent height estimated by OMI-MODIS between the surface to  $\sim 2$ km.  
389 In this range, it was seen that the height assumed by OMI is  $> 1.5$ km compared to the one  
390 estimated by OMI-MODIS. Thus, OMI overestimated SSA compared to OMI-MODIS retrieval.  
391 Gassó and Torres (2016), in their detailed analysis of the OMI UV aerosol product (version

392 1.4.2), studied the OMI-MODIS method for two specific cases. They have mentioned that when  
393 the extrapolated MODIS 388nm AOD was not within the OMI LUT values, the OMI-MODIS  
394 algorithm retrieves unrealistic height and SSA. For the ARBOB region, the difference in AOD  
395 ( $AOD_{MODIS} - AOD_{OMI}$ ) has been plotted with the difference in SSA ( $SSA_{OMI-MODIS} - SSA_{OMI}$ )  
396 (Fig. 6b). The colorbar represents the difference in ALH ( $ALH_{OMI-MODIS} - ALH_{OMI}$ ) retrieved by  
397 both the algorithms. An inverse relation was seen implying that when OMI underestimated AOD  
398 compared to MODIS, OMI overestimated SSA compared to OMI-MODIS. The difference in  
399 AOD was mainly within the  $\pm 0.5$  range. However, there are a few points where the AOD  
400 difference was  $>3$ . Mostly in such cases, the difference between the ALH and SSA estimates of  
401 both the algorithms was high. However, there are points when the AOD difference was high and  
402 the ALH and SSA differences were within  $\pm 1$  km and  $\pm 0.03$  respectively. Similarly, the  
403 difference between ALH and SSA values of both the algorithms was high when the AOD  
404 difference was within  $\pm 0.5$ . These discrepancies could be attributed to the AOD spectral  
405 curvature of an aerosol type assumed by MODIS which is different from the aerosol model  
406 assumed by OMI UV aerosol product (Gassó and Torres, 2016). Whether any other property  
407 apart from AOD and shape (for dust aerosols) can affect the ALH and SSA retrievals have to be  
408 studied in the future.

409 The importance of ALH and SSA in the calculation of TOA flux was studied using the Santa  
410 Barbara DISORT (SBDART) model (Ricchiazzi et al., 1998). For the same tropical environment  
411 variables and surface albedo of 0.06, the SSA was varied from 0.8 to 1 and aerosol height from 0  
412 to 10 km at 1 km interval. The simulations were done for a narrow band in UV (300-400nm). For  
413 a constant AOD, AE (Angstrom Exponent) and asymmetry factor (0.4, 1 and 0.7 respectively),  
414 TOA flux was calculated (Fig. 7a). It can be seen that at any ALH, TOA flux varied with SSA.

415 The role of ALH is important in the UV region due to the phenomena of Rayleigh scattering (van  
416 de Hulst, 1981). The importance of Rayleigh scattering on the role of ALH is further shown in  
417 Fig. 7b. In this particular set of simulations, the Rayleigh scattering is completely removed and  
418 all other parameters are kept the same as in Fig. 7a. It can be seen that once molecular scattering  
419 is removed, the effect of ALH is also removed and TOA flux depends only on SSA and other  
420 aerosol properties. The basis of many aerosol retrievals by satellites in the UV spectrum is the  
421 sensitivity of aerosol absorption to Rayleigh scattering which acts as a bright background and  
422 contributes to the TOA radiance (Torres et al., 1998; 2002). Change in ALH can affect the TOA  
423 radiance since the aerosol layer will interact with the Rayleigh scattering due to molecules  
424 present in the atmosphere. However, this effect is smaller compared to the effect due to the  
425 change in AOD and SSA (Kim et al., 2018). Kim et al. (2018) also showed how the  
426 misclassification of aerosol type and size could affect ALH retrieval. OMI SSA retrievals which  
427 are based on LUT depend on the ALH assumed along with aerosol type. The SBDART  
428 simulations in the current work show how for a particular TOA flux, SSA varies with ALH when  
429 the other aerosol properties are kept constant.

#### 430 **5.4. Comparison between SSA retrievals from OMI and OMI-MODIS with ship-borne** 431 **estimates.**

432 To validate the new retrieval method of SSA using OMI and MODIS, both SSA values from  
433 OMI and OMI-MODIS were compared with ground-based measurements (SSA at 450nm)  
434 during cruises in the period 2006 and 2009 in the Arabian Sea and Bay of Bengal. These cruises  
435 were part of the Integrated Campaign for Aerosols, gases and Radiation Budget (ICARB)  
436 performed during March to May 2006 and once during winter (W-ICARB) from 27 December  
437 2008 to 30 January 2009 (Moorthy et al., 2008 and 2010). During both the cruises the aerosol

438 sampling was done onboard the Oceanic Research Vessel *Sagar Kanya*. While the 2006 cruise  
439 covered both the Arabian Sea and the Bay of Bengal, the winter cruise of 2009 covered the Bay  
440 of Bengal. The cruise tracks are provided in detail in Moorthy et al., 2008 and 2010, respectively.  
441 The SSA values at different wavelengths were estimated from spectral values of the absorption  
442 coefficient and scattering coefficient measured using the instruments Aethalometer (Magee  
443 Scientific AE-31, USA) and an integrating nephelometer (TSI 3563, USA) respectively. More  
444 details about the instrument and measuring techniques including the uncertainties are provided in  
445 Nair et al. (2008). However, both the cruise did not estimate SSA values in the UV spectrum. The  
446 closest wavelength at which SSA is calculated is 450nm which has been used to compare with  
447 the satellite retrievals of SSA (388nm). Ground-based SSA estimates based on in-situ  
448 measurements are seldom consistent with columnar satellite retrievals especially when elevated  
449 aerosols are present. This uncertainty along with the uncertainty in the assumption of SSA being  
450 uniform between 388nm and 450nm implies that the current comparison of study cannot be used  
451 as a validation study. Instead, it is used to understand the consistency of SSA retrievals from  
452 satellites with ground-based observations. Since the cruise measurements had little coverage  
453 spatially, for better coverage, a 2° box was used around each location within which the mean  
454 SSA was calculated for the respective cruise period. These values are plotted in Fig. 8. Circle and  
455 square markers represent OMI and OMI-MODIS comparison respectively. It can be seen that  
456 despite using a 2° box, the number of points having valid SSA values for the cruise and the  
457 satellite retrievals was only 21. This number increased as the size of the box around each cruise  
458 location was increased. The low number is due to the sparse nature of the OMI-MODIS retrieval  
459 over the region (Fig. 1b). The colour scale represents the cruise and the region where the aerosol  
460 sampling was taken.

461 During the ICARB, the presence of elevated aerosols at a height of ~1km-3km have been  
462 shown in earlier studies (Satheesh et al., 2008; Nair et al., 2009). In such cases comparison  
463 between a ship-based aerosol retrieval which detects aerosols close to the surface and the SSA  
464 retrieval from satellites which detects these elevated aerosols cannot be considered appropriate.  
465 This discrepancy was seen in Fig. 8 especially over the Arabian Sea (Blue colour) and some  
466 points over Bay of Bengal (Red). In some cases, OMI was able to retrieve SSA consistent with  
467 the cruise estimated, unlike OMI-MODIS. This could be due to the improvement of dust model  
468 assumption in the new version of OMI aerosol product and (or) due to the wrong spectral AOD  
469 dependence assumed by MODIS. During the winter most of the aerosols influencing the Bay of  
470 Bengal is present closer to the surface. In such cases comparing the SSA estimates can be valid.  
471 It was observed that during winter when aerosols are generally present close to the surface, OMI-  
472 MODIS retrieved SSA which is a bit more consistent with the ship estimates compared to OMI.  
473 In such cases, OMI still overestimated SSA despite the improvement in the algorithm. The  
474 respective RMSEs for OMI and OMI-MODIS comparison with the cruise estimates were 0.05  
475 and 0.06. Due to the lack of common points, the correlation was also poor (OMI-MODIS: 0.11  
476 and OMI: -0.35).

477

478 The OMI-MODIS approach in SSA retrieval is one of the many combinations of sensors that  
479 can be used in retrieving aerosol properties. A better approach involving the vertical distribution  
480 of aerosols either from space or ground-based observations is required to reduce the uncertainty  
481 further. However, with few ground-based measurements in the UV regime especially over the  
482 oceans and fewer retrievals of the vertical aerosol absorption, validation of new algorithms is  
483 still in the nascent stage.

## 484 6. Summary and Conclusions

485 Aerosol forcing depends on aerosol properties such as aerosol optical depth (AOD) and  
486 single scattering albedo (SSA). SSA is highly sensitive to the aerosol composition, size and the  
487 wavelength at which the aerosol interacts with radiation. A slight change in SSA value can alter  
488 the sign of the forcing. Hence it is important to have an accurate measurement of SSA globally.  
489 The Ozone Monitoring Instrument (OMI) retrieves SSA in the UV spectrum. However, these  
490 retrievals might be affected by the cloud contamination due to the coarser pixel resolution of 13  
491 x 24 km<sup>2</sup> and are sensitive to the assumption of aerosol layer height in the inversion procedure.  
492 In addition to these problems, uncertainty in the surface albedo is a source of error for SSA  
493 retrieval. To resolve the issue of sub-pixel cloud contamination, Satheesh et al. (2009) developed  
494 a method using the combination of OMI and the Moderate Resolution Imaging  
495 Spectroradiometer (MODIS) at a local scale. In the present study, we used the method developed  
496 by Satheesh et al. (2009) to retrieve SSA at a much larger spatial and temporal scales. The main  
497 findings from our study are listed below:

- 498 1. Both OMI and OMI-MODIS algorithms retrieved SSA over regions influenced by large  
499 amounts of aerosols with moderate to high absorption capacity (e.g. Atlantic Ocean –  
500 ATL; Arabian Sea and Bay of Bengal – ARBOB)
- 501 2. The difference in SSA retrievals of both the algorithms ( $\Delta$ SSA) was found to be within  
502  $\pm 0.03$  over ATL for more than 80% of the time during all the seasons. Over the Arabian  
503 Sea, as seen in Satheesh et al. (2009),  $\Delta$ SSA was within the  $\pm 0.03$  range during MAM  
504 when the region was influenced by dust. The discrepancy during other season was due to  
505 the wrong assumption of aerosol layer height by OMI. The discrepancy in SSA could  
506 also be partly attributed to the sub-pixel cloud contamination during the summer

507 monsoon season.

508 3. From Fig. 6a it was seen that OMI overestimated SSA when it overestimated ALH and  
509 vice versa. This could be attributed to the wrong assumption of aerosol height. Fig. 6b  
510 showed that difference in AOD and difference in SSA had an inverse relationship.  
511 Further analysis on whether any other factor apart from ALH and aerosol shape can affect  
512 SSA retrieval has to be studied.

513 4. Both SSA retrievals were compared with cruise data from the ICARB and W-ICARB  
514 campaigns in the Arabian Sea and Bay of Bengal.

515 5. While both the algorithms did not match the cruise estimate during most of the dust  
516 season due to the presence of elevated aerosols not sampled by surface instrument, in few  
517 cases during ICARB, OMI performed better than OMI-MODIS. This could be due to the  
518 better assumption of dust model in the algorithm and/or wrong model assumption by  
519 MODIS. During winter, when the aerosols were present closer to the surface, OMI-  
520 MODIS was a bit more consistent compared to OMI. This may be due to scenarios where  
521 the CALIPSO climatology was absent and OMI used its previous aerosol model  
522 assumptions. This could also be due to uncertainties in ALH value even after the  
523 improvement in the OMI algorithm with the addition of CALIPSO climatology.

524 OMI retrieves aerosol properties at high cloud fraction (Gassó and Torres, 2016) implying  
525 two things, either OMI is able to detect aerosols present above clouds or the OMI pixel was  
526 prone to cloud contamination. In their study, Gassó and Torres (2016), observed that while  
527 MODIS cloud fraction could be used to screen out cloudy pixels in OMI, it could not be the lone  
528 criterion. While they performed for a single case, an analysis of a larger spatial and temporal  
529 scale is required. Aerosol type and aerosol layer height play a vital role in the retrieval of aerosol

530 properties. Without the assumption of aerosol type or height, OMI-MODIS provided SSA  
531 retrievals which were consistent with cruise estimates during the winter when the Bay of Bengal  
532 was influenced by anthropogenic aerosols present close to the surface. This was not the case  
533 when dust aerosols were present. This discrepancy can be attributed to the difference in the  
534 aerosol model assumption by MODIS and OMI. This comparison study had very few points for a  
535 detailed analysis. Hence, an accurate comparison and validation of such retrieval algorithms can  
536 be possible only when there are more ground-based observations available in the UV spectrum  
537 on a larger spatial and temporal scale along with vertical profiles of aerosol absorption.

### 538 **Author Contributions**

539 KE downloaded, prepared and performed the data analysis under the supervision of SKS and JS.  
540 All the authors contributed to the interpretation and the discussion of the analysis and the results  
541 as well as the writing of the paper.

### 542 **Acknowledgements**

543 The authors gratefully acknowledge the NOAA Air Resources Laboratory (ARL) for the  
544 provision of the HYSPLIT transport and dispersion model used in this publication. The authors  
545 are grateful to NASA data and services centre.

### 546 **References**

- 547 Bergstrom, R.W., Pilewskie, P., Russell, P.B., Redemann, J., Bond, T.C., Quinn, P.K., and Sierau,  
548 B.: Spectral absorption properties of atmospheric aerosols, *Atmos. Chem. Phys.*, 7, 5937-  
549 5943, 2007.
- 550 Bond, T.C., and Sun, H.: Can reducing black carbon emissions counteract global warming?,  
551 *Environ. Sci. Technol.*, 39(16), 5921-5926, 2005.
- 552 Bond, T.C., and Bergstrom, R.W.: Light absorption by carbonaceous particles: An investigative



553 review, *Aerosol Sci. Tech.*, 40(1), 27-67, doi:10.1080/02786820500421521, 2006.

554 Bond, T.C., Doherty, S.J., Fahey, D.W., Forster, P.M., Bernsten, T., De Angelo, B.J., Flanner,  
555 M.G., Ghan, S., Karcher, B., Koch, D., Kinne, S., Kondo, Y., Quinn, P.K., Sarofim, M.C.,  
556 Schultz, M., Venkataraman, C., Zhang, H., Zhang, S., Bellouin, N., Guttikunda, S.K.,  
557 Hopke, P.K., Jacobson, M.Z., Kaiser, J.W., Klimont, Z., Lohmann, U., Schwarz, J.P.,  
558 Shindell, D., Storelvmo, T., Warren, S.G., and Zender, C.S.: Bounding the role of black  
559 carbon in the climate system: A scientific assessment, *J. Geophys. Res.*, 118(11), 5380-  
560 5552, doi:10.1002/jgrd.50171, 2013.

561 Chand, D., Wood, R., Anderson, T.L., Satheesh, S.K., and Charlson, R.J.: Satellite-derived direct  
562 radiative effect of aerosols dependent on cloud cover, *Nat. Geosci.*, 2, 181–184,  
563 doi:10.1038/ngeo437, 2009.

564 Chung, S.H., and Seinfeld, J.H.: Global distribution and climate forcing of carbonaceous  
565 aerosols, *J. Geophys. Res.*, 107(D19), 4407, doi:10.1029/2001JD001397, 2002.

566 Cooke, W.F., and Wilson, J.J.N.: A global black carbon aerosol model, *J. Geophys. Res.*, 101,  
567 19395-19410, doi:10.1029/96JD00671, 1996.

568 Dey, S., and Di Girolamo, L.: A climatology of aerosol optical and microphysical properties over  
569 the Indian subcontinent from 9 years (2000–2008) of Multiangle Imaging  
570 Spectroradiometer (MISR) data, *J. Geophys. Res.*, 115, D15204,  
571 doi:10.1029/2009JD013395, 2010.

572 Di Girolamo, L., Bond, T.C., Bramer, D., Diner, D.J., Fettingner, F., Kahn, R.A., Mrtonchik, J.V.,  
573 Ramana, M.V., Ramanathan, V., and Rasch, P.J.: Analysis of Multi-angle Imaging  
574 SpectroRadiometer (MISR) aerosol optical depths over greater India during winter 2001-  
575 2004, *Geophys. Res. Lett.*, 31(23), L23115, doi:10.1029/2004GL021273, 2004.

576 Diner, D.J., Beckert, J.C., Reilly, T.H., Bruegge, C.J., Conel, J.E., Kahn, R.A., Martonchik, J.V.,  
577 Ackerman, T.P., Davies, R., Gerstl, S.A.W., Gordon, H.R., Muller, J.-P., Myneni, R.B.,  
578 Sellers, P.J., Pinty, B., and Verstraete, M.M.: Multi-angle Imaging SpectroRadiometer  
579 (MISR) instrument description and experiment overview, *IEEE T GEOSCI REMOTE*,  
580 36(4), 1072-1087, doi:10.1109/36.700992, 1998.

581 Dubovik, O., and King, M.D.: A flexible inversion algorithm for retrieval of aerosol optical  
582 properties from Sun and sky radiance measurements, *J. Geophys. Res.*, 105(D16), 20673-  
583 20696, doi:10.1029/2000JD900282, 2000.

584 Dubovik, O., Holben, B.N., Eck, F.T., Smirnov, A., Kaufman, Y.J., King, M.D., Tanré, D., and  
585 Slutsker, I.: Variability of absorption and optical properties of key aerosol types observed  
586 in worldwide locations, *J. Atmos. Sci.*, 59(3), 590-608, doi:10.1175/1520-  
587 0469(2002)059<0590:VOAAOP>2.0.CO;2, 2002.

588 Eck, T.F., Holben, B.N., Slutsker, I., and Setzer, A.: Measurements of irradiance attenuation and  
589 estimation of aerosol single scattering albedo for biomass burning aerosols in Amazonia, *J.*  
590 *Geophys. Res.*, 103(D24), 31865-31878, doi:10.1029/98JD00399, 1998.

591 Gassó, S., and Torres, O.: The role of cloud contamination, aerosol layer height and aerosol  
592 model in the assessment of the OMI near-UV retrievals over the ocean, *Atmos. Meas.*  
593 *Tech.*, 9, 3031-3052, doi:10.5194/amt-9-3031-2016, 2016.

594 Hansen, J., Sato, M., and Ruedy, R.: Radiative forcing and climate response, *J. Geophys. Res.-*  
595 *Atmos.*, 102(D6), 6831-6864, doi:10.1029/96JD03436, 1997.

596 Harriss, R.C., Browell, E.V., Sebacher, D.I., Gregory, G.L., Hinton, R.R., Beck, S.M., McDougal,  
597 D.S., and Shipley, S.T.: Atmospheric transport of pollutants from North America to the  
598 North Atlantic Ocean, *Nature*, 308, 722-724, doi:10.1038/308722a0, 1984.

599 Haywood, J.M., Roberts, D.L., Slingo, A., Edwards, J.M., and Shine, K.P.: General circulation  
600 model calculations of the direct radiative forcing by anthropogenic sulphate and fossil-fuel  
601 soot aerosol, *J. Clim.*, 10, 1562-1577, doi:10.1175/1520-  
602 0442(1997)010<1562:GCMCOT>2.0.CO;2, 1997.

603 Heintzenberg, J., Charlson, R.J., Clarke, A. D., Liousse, C., Ramaswamy, V., Shine, K.P.,  
604 Wendish, M., and Helas, G: Measurements and modelling of aerosol single-scattering  
605 albedo: Progress, problems and prospects, *Contrib. Atmos. Phys.*, 70(4), 249– 263, 1997.

606 Herman, B.M., Browning, R.S., and De Luisi, J.J.: Determination of the effective imaginary term  
607 of the complex refractive index of atmospheric dust by remote sensing: the diffuse-direct  
608 radiation method, *J. Atmos. Sci.*, 32, 918-925, doi:10.1175/1520-  
609 0469(1975)032<0918:DOTEIT>2.0.CO;2, 1975.

610 Herman, J.R., Bhartia, P.K., Torres, O., Hsu, C., Seftor, C., and Celarier, E.: Global distribution  
611 of UV-absorbing aerosols from Nimbus 7/TOMS data, *J. Geophys. Res.-Atmos.*, 102(D14),  
612 16911-16922, doi:10.1029/96JD03680, 1997.

613 Horvath, H.: Atmospheric light absorption- a review, *Atmos. Environ. A-Gen.*, 27(3), 293-317,  
614 doi:10.1016/0960-1686(93)90104-7, 1993.

615 Intergovernmental Panel on Climate Change (IPCC) (2013), The physical science basis:  
616 Contribution of Working Group I to the Fifth Assessment Report of the Intergovernmental  
617 Panel on Climate Change, In: *Climate Change (2013)*, Stocker, T.F., D. Qin, G.K. Plattner,  
618 M. Tignor, S.K. Allen, J. Boschung, A. Nauels, Y. Xia, V. Bex, and P.M. Midgley (eds),  
619 Cambridge University, Press: Cambridge, United Kingdom and New York, NY, USA 1535  
620 pp, doi:10.1017/CBO9781107415324.

621 Jethva, H., Torres O., and Ahn C.: Global assessment of OMI aerosol single-scattering albedo

622 using ground-based AERONET inversion, *J. Geophys. Res.-Atmos.*, 119(14), 9020-9040,  
623 doi:10.1002/2014JD021672, 2014.

624 Johnson, B.T., Shine, K.P., and Forster, P.M.: The semi-direct aerosol effect: Impact of absorbing  
625 aerosols on marine stratocumulus, *Q. J. Roy. Meteor. Soc.*, 130, 1407-1422,  
626 doi:10.1256/qj.03.61, 2003.

627 Kaufman, Y.J.: Satellite sensing of aerosol absorption, *J. Geophys. Res.*, 92, 4307-4317,  
628 doi:10.1029/JD092iD04p04307, 1987.

629 Kaufman, Y.J., Tanré, D., and Boucher, O.: A satellite view of aerosols in the climate system,  
630 *Nature*, 419, 215-223, doi:10.1038/nature01091, 2002a.

631 Kaufman, Y.J., Martins, J.V., Remer, L.A., Schoeberl, M.R., and Yamasoe, M.A.: Satellite  
632 retrieval of aerosol absorption over the oceans using sunglint, *Geophys. Res. Lett.*, 29(19),  
633 34-1 – 34-4, doi:10.1029/2002GL015403, 2002b.

634 Kaufman, Y.J., Koren, I., Remer, L.A., Tanré, D., Ginoux, P., and Fan, S.: Dust transport and  
635 deposition observed from the Terra-Moderate Resolution Imaging Spectroradiometer  
636 (MODIS) spacecraft over the Atlantic Ocean, *J. Geophys. Res.*, 110, D10S12,  
637 doi:10.1029/2003JD004436, 2005.

638 Kim, S-W., Yoon, S-C., Jefferson, A., Won, J-G, Dutton, E.G., Ogren, J.A., and Anderson T.L.:  
639 Observation of enhanced water vapour in Asian dust layer and its effect on atmospheric  
640 radiative heating rates, *Geophys. Res. Lett.*, 31(18), doi:10.1029/2004GL020024, 2004.

641 Kim, M., Kim, J., Torres, O., Ahn, C., Kim, W., Jeong, U., Go, S., Liu X., Moon, K.J., and Kim,  
642 D.-R.: Optimal Estimation-Based Algorithm to Retrieve Aerosol Optical Properties for  
643 GEMS Measurements over Asia, *Remote Sens.*, 10(2), 162, doi:10.3390/rs10020162, 2018.

644 King, M.D.: Determination of the ground albedo and the index of absorption of atmospheric

645 particulates by remote sensing. Part II: Application, *J. Atmos. Sci.*, 36, 1072-1083,  
646 doi:10.1175/1520-0469(1979)036<1072:DOTGAA>2.0.CO;2, 1979.

647 Krishnamurti, T.N., Jha, B., Prospero J., Jayaraman, A., and Ramanathan, V.: Aerosol and  
648 pollutant transport and their impact on radiative forcing over the tropical Indian Ocean  
649 during the January – February 1996 pre-INDOEX cruise, *Tellus B*, 50(5): 521–542,  
650 doi:10.1034/j.1600-0889.1998.00009.x, 1998.

651 Kumar, K.R., Sivakumar, Reddy, R.R., and Gopal, K.R.: Ship-borne measurements of columnar  
652 and surface aerosol loading over the Bay of Bengal during W-ICARB campaign: role of  
653 air mass transport. Latitudinal and Longitudinal Gradients, *Aerosol Air Qual Res.*, 13, 818–  
654 837, doi:10.4209/aaqr.2012.08.0225, 2013.

655 Lawrence, M.G., and Lelieveld, J.: Atmospheric pollutant outflow from southern Asia: a review,  
656 *Atmospheric Chemistry and Physics*, 10, 11017-11096, doi:10.5194/acp-10-11017-2010,  
657 2010.

658 Levy, R.C., Remer, L.A., Tanré, D., Kaufman, Y.J., Ichoku, C., Holben, B.N., Livingston, J.M.,  
659 Russell, P.B., and Maring, H.: Evaluation of the Moderate-Resolution Imaging  
660 Spectroradiometer (MODIS) retrievals of dust aerosol over the ocean during PRIDE, *J.*  
661 *Geophys. Res.*, 108(D19), 8594, doi:10.1029/2002JD002460, 2003.

662 Levy, R.C., Mattoo, S., Munchak, L.A., Remer, L.A., Sayer, A.M., Patadia, F., and Hsu N.C.:  
663 The collection 6 MODIS aerosol products over land and ocean, *Atm. Meas. Tech.*, 6, 2989-  
664 3034, doi:10.5194/amt-6-2989-2013, 2013.

665 Liao, H., and Seinfeld, J.H.: Radiative forcing by mineral dust aerosols: Sensitivity to key  
666 variables, *J. Geophys. Res.-Atmos.*, 103(D24), 31637-31645, doi:10.1029/1998JD200036,  
667 1998.

668 Meloni, D., di Sarra, A., di Lorio, T., and Fiocco, G.: Influence of the vertical profile of Saharan  
669 dust on the visible direct radiative forcing, *J. Quant. Spectrosc. Ra.*, 93(4), 397-413,  
670 doi:10.1016/j.jqsrt.2004.08.035, 2005.

671 Menon, S., Hansen, J., Nazarenko, L., and Luo, Y.: Climate effects of black carbon aerosols in  
672 China and India, *Science*, 297(5590), 2250-2253, doi:10.1126/science.1075159, 2002.

673 Mishra, A.K., Koren, I., and Rudich, Y.: Effect of aerosol vertical distribution on aerosol-  
674 radiation interaction: A theoretical prospect, *Heliyon*, e00036,  
675 doi:10.1016/j.heliyon.2015.e00036, 2015.

676 Moorthy, K.K., Babu, S.S., and Satheesh, S.K.: Aerosol spectral optical depths over the Bay of  
677 Bengal: role of transport, *Geophys. Res. Lett.*, 30(5): 1249, doi:10.1029/2002GL016520,  
678 2003.

679 Moorthy, K.K., Babu, S.S., Sunilkumar, S.V., Gupta, P.K., and Gera, B.S.: Altitude profiles of  
680 aerosol BC, derived from aircraft measurements over an inland urban location in India,  
681 *Geophys. Res. Lett.*, 31(22), 10.1029/2004GL021336, 2004.

682 Moorthy, K.K., Satheesh, S.K., Babu, S.S., and Dutt, C.B.S.: Integrated campaign for aerosols,  
683 gases and radiation budget (ICARB): an overview, *J. Earth. Syst. Sci.*, 117(1), 243-262,  
684 doi:10.1007/s12040-008-0029-7, 2008.

685 Moorthy, K.K., Beegum, S.N., Babu, S.S., Smirnov, A., John, S.R., Kumar, K.R., Narasimhulu,  
686 K., Dutt, C.B.S., and Nair, V.S.: Optical and physical characteristics of Bay of Bengal  
687 aerosols during W-ICARB: spatial and vertical heterogeneities in the marine atmospheric  
688 boundary layer and in the vertical column, *J. Geophys. Res.*, 115(D24): D24213,  
689 doi:10.1029/2010JD014094, 2010.

690 Moosmuller, H., Chakrabarty, R.K., and Arnott, W.P.: Aerosol light absorption and its

691 measurement: A review, *J. Quant. Spectrosc. Ra.*, 110(11), 844-878,  
692 doi:10.1016/j.jqsrt.2009.02.035, 2009.

693 Morris, V., Colon, P.C., Nalli, N.R., Joseph, E., Armstrong, R.A., Detres, Y., Goldberg, M.D.,  
694 Minnett, P.J., and Lumpkin, R.: Measuring Trans-Atlantic aerosol transport from Africa,  
695 *EOS Trans. AGU*, 87(50), 565-571, doi:10.1029/2006EO500001, 2006.

696 Myhre, G., Stordal, F., Restad, K., and Isaksen, I.S.A.: Estimation of the direct radiative forcing  
697 due to sulphate and soot aerosols, *Tellus*, 50B, 463-477, 1998.

698 Nair, V.S., Babu, S.S., and Moorthy, K.K.: Spatial distribution and spectral characteristics of  
699 aerosol single scattering albedo over the Bay of Bengal inferred from shipborne  
700 measurements, *Geophys. Res. Lett.*, 35, doi:10.1029/2008GL033687, 2008.

701 Nair V.S., Moorthy, K.K., and Babu, S.S.: Optical and Physical Properties of Atmospheric  
702 Aerosols over the Bay of Bengal during ICARB, *J. Atmos. Sci.*, 66, doi:  
703 10.1175/2009JAS3032.1, 2009.

704 Narasimhan, D., and Satheesh, S.K.: Estimates of aerosol absorption over India using multi-  
705 satellite retrieval, *Ann. Geophys.*, 31, 1773-1778, doi:10.5194/angeo-31-1773-2013, 2013.

706 Pease, P.P., Tchakerian, V.P., and Tindale, N.W.: Aerosols over the Arabian Sea: geochemistry  
707 and source areas for Aeolian desert dust, *J. Arid Environ.*, 39(3), 477-496,  
708 doi:10.1006/jare.1997.0368, 1998.

709 Podgorny, I.A., and Ramanathan, V.: A modeling study of the direct effect of aerosols over the  
710 tropical Indian Ocean, *J. Geophys. Res.*, 106(D20): 24097–24105,  
711 doi:10.1029/2001JD900214, 2001.

712 Prospero, J.M., and Carlson, T.N.: Vertical and areal distribution of Saharan dust over the  
713 western equatorial north Atlantic Ocean, *J. Geophys. Res.*, 77(27), 5255-5265,

714 doi:10.1029/JC077i027p05255, 1972.

715 Prospero, J.M.: Saharan dust transport over the North Atlantic Ocean and Mediterranean: An  
716 overview, In: *The Impact of Desert Dust Across the Mediterranean*, Guerzoni S., Chester  
717 R. (Eds.), 133-151, doi:10.1007/978-94-017-3354-0\_13, 1996.

718 Rajeev, K., Ramanathan, V., and Meywerk, J.: Regional aerosol distribution and its long-range  
719 transport over the Indian Ocean, *J. Geophys. Res.-Atmos.*, 105(D2), 2029-2043,  
720 doi:10.1029/1999JD900414, 2000.

721 Ramanathan, V., Crutzen, P.J., Kiehl, J.T., and Rosenfield, D.: Aerosols, climate and the  
722 hydrological cycle, *Science*, 294(5549): 2119–2124, doi:10.1126/science.1064034, 2001.

723 Remer, L. A., Kaufman, Y. J., Tanré, D., Mattoo, S., Chu, D. A., Martins, J. V., Li, R. R., Ichoku,  
724 C., Levy, R. C., Kleidman, R. G., Eck, T. F., Vermote, E., and Holben, B. N.: The MODIS  
725 aerosol algorithm, products, and validation, *J. Atmos. Sci.*, 62, 947–973,  
726 doi:10.1175/JAS3385.1, 2005.

727 Ricchiuzzi, P., Yang, S., Gautier, C., and Sowle, D.: SBDART: a research and teaching software  
728 tool for plane-parallel radiative transfer in the earth’s atmosphere, *B. Am. Meteorol. Soc.*  
729 79(10): 2101–2114, doi:10.1175/1520-0477(1998)079<2101: SARATS>2.0.CO;2, 1998.

730 Satheesh, S.K.: Aerosols and climate, *Resonance*, 7(4), 48-59, doi:10.1007/BF02836138, 2002.

731 Satheesh, S.K., and Moorthy, K.K.: Radiative effects of natural aerosols: a review, *Atmos.*  
732 *Environ.*, 39(11): 2089–2110, doi:10.1016/j.atmosenv.2004.12.029, 2005.

733 Satheesh, S.K., Srinivasan, J., and Moorthy, K.K.: Spatial and temporal heterogeneity in aerosol  
734 properties and radiative forcing over Bay of Bengal: Sources and role of aerosol transport,  
735 *J. Geophys. Res.*, 111(D8): D08202, doi:10.1029/2005JD006374, 2006.

736 Satheesh, S.K., Moorthy, K.K., Babu, S.S., Vinoj, V., and Dutt, C.B.S.: Climate implications of



737 large warming by elevated aerosol over India, *Geophys. Res. Lett.*, 35(19),  
738 doi:10.1029/2008GL034944, 2008.

739 Satheesh, S.K., Torres, O., Remer, L.A., Babu, S.S., Vinoj, V., Eck, T.F., Kleidman, R.G., and  
740 Holben, B.N.: Improved assessment of aerosol absorption using OMI-MODIS joint  
741 retrieval, *J. Geophys. Res.*, 114, D05209, doi:10.1029/2008JD011024, 2009.

742 Satheesh, S.K., Vinoj, V., and Moorthy, K.K.: Assessment of aerosol radiative impact over  
743 oceanic regions adjacent to Indian subcontinent using multi-satellite analysis, *Adv.*  
744 *Meteorol.*, 2010, Article ID 139186, pp 13., doi:10.1155/2010/139186, 2010.

745 Seinfeld, J.H., and Pandis, S.N.: *Atmospheric Chemistry and Physics: From air pollution to*  
746 *climate change*, 2nd Ed., 1232 pp, John Wiley & Sons, Inc., Hobkoben, New Jersey, 2006.

747 Sirocko, F., and Sarnthein, M.: Wind-borne deposits in the northwestern Indian Ocean: Record of  
748 Holocene sediments versus modern satellite data, In: *Paleoclimatology and*  
749 *Paleometeorology: modern and past patterns of global atmospheric transport*, Leinen M.,  
750 Sarnthein M. (Eds), 401-433, Amsterdam: Kluwer Academic Publishers, 1989.

751 Stephens, G.L., Vane, D.G., Boain, R.J., Mace, G.G., Sassen, K., Wang, Z., Illingworth, A.J.,  
752 O'Connor, E.J., Rossow, W.B., Durden, S.L., Miller, S.D., Austin, R.T., Benedetti, A.,  
753 Mitrescu, C., and CloudSat Science Team: The CloudSat mission and the A-Train: A new  
754 dimension of space-based observations of clouds, precipitation, *B. Am. Meteorol. Soc.*, 83,  
755 1771-1790, doi:10.1175/BAMS-83-12-1771, 2002.

756 Tanré, D., Kaufman, Y.J., Herman, M., and Mattoo, S.: Remote sensing of aerosol properties  
757 over oceans using the MODIS/EOS spectral radiances, *J. Geophys. Res.*, 102(D14),  
758 16971–16988, 1997.

759 Tindale, N.W., and Pease, P.P.: Aerosols over the Arabian Sea: Atmospheric transport pathways

760 and concentrations of dust and sea salt, *Deep-Sea Res. Pt. II*, 46(8-9), 1577-1595,  
761 doi:10.1016/S0967-0645(99)00036-3, 1999.

762 Torres, O., Bhartia, P. K., Herman, J. R., and Ahmad, Z.: Derivation of aerosol properties from  
763 satellite measurements of backscattered ultraviolet radiation. *Theoretical Basis*, *J.*  
764 *Geophys. Res.*, 103(D14), 17099–17110, 1998.

765 Torres, O., Decae, R., Veefkind, J.P., and de Leeuw, G.: OMI aerosol retrieval algorithm, in *OMI*  
766 *Algorithm Theoretical Basis Document: Clouds, Aerosols, and Surface UV Irradiance*, 3,  
767 *V2*, OMIATBD- 03, edited by P. Stammes, pp. 47 – 71, NASA Goddard Space Flight  
768 *Cent.*, Greenbelt, Md, 2002.  
769 ([http://eosps0.gsfc.nasa.gov/eos\\_homepage/for\\_scientists/atbd/docs/OMI/ATBD-OMI-](http://eosps0.gsfc.nasa.gov/eos_homepage/for_scientists/atbd/docs/OMI/ATBD-OMI-03.pdf)  
770 [03.pdf](http://eosps0.gsfc.nasa.gov/eos_homepage/for_scientists/atbd/docs/OMI/ATBD-OMI-03.pdf))

771 Torres, O., Bhartia, P.K., Sinyuk, A., Welton, E.J., and Holben, B.: Total Ozone Mapping  
772 Spectrometer measurements of aerosol absorption from space: Comparison to SAFARI  
773 2000 ground-based observations, *J. Geophys. Res.*, 110(D10), doi:10.1029/2004JD004611,  
774 2005.

775 Torres, O., Tanskanen, A., Veihelmann, B., Ahn, C., Braak, R., Bhartia, P.K., Veefkind, P., and  
776 Levelt, P.: Aerosols and surface UV products from Ozone Monitoring Instrument  
777 observations: An overview, *J. Geophys. Res.*, 112, D24S47, doi:10.1029/2007JD008809,  
778 2007.

779 Torres, O., Ahn, C., and Chen, Z.: Improvements to the OMI near-UV aerosol algorithm using A-  
780 train CALIOP and AIRS observations, *Atmos. Meas. Tech.*, 6, 3257-3270,  
781 doi:10.5194/amt-6-3257-2013, 2013.

782 Torres, O., Bhartia, P.K., Jethva, H., and Ahn, C.: Impact of the ozone monitoring instrument row

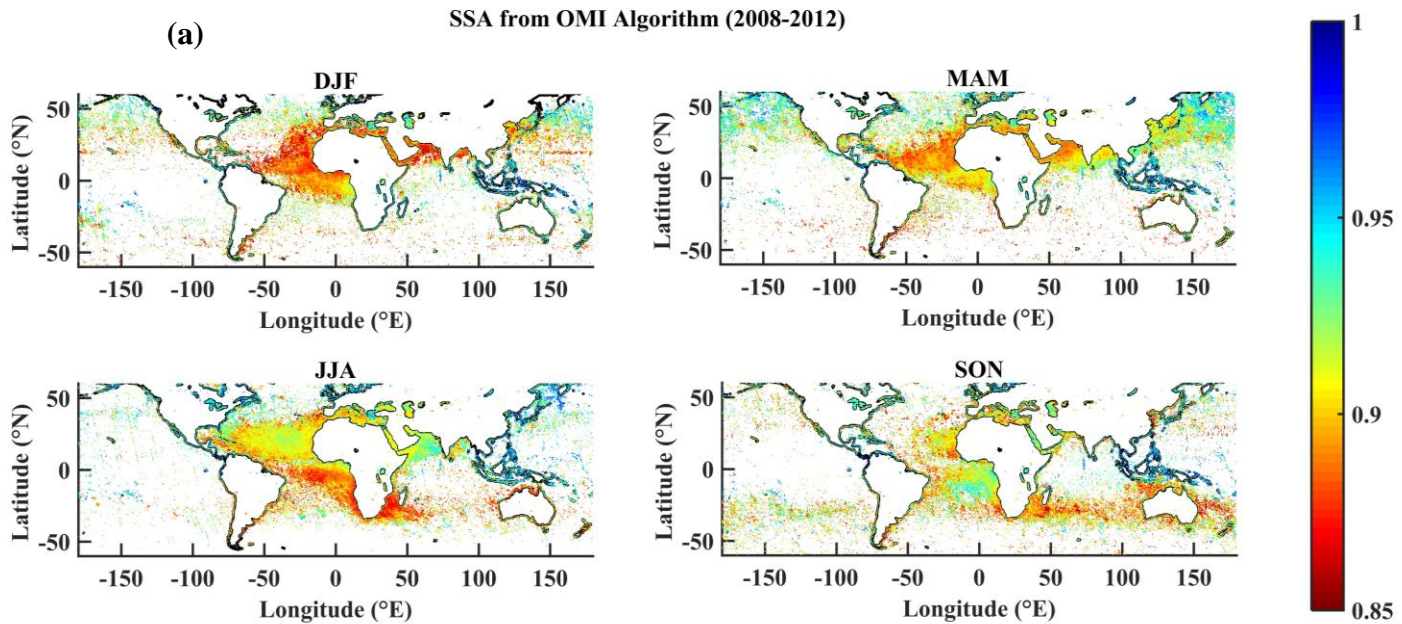
783 anomaly on the long-term record of aerosol products, *Atmos. Meas. Tech.*, 11, 2701-2715,  
 784 doi:10.5194/amt-11-2701-2018, 2018.

785 Van de Hulst, H.C.: *Light scattering by small particles*, 496 pp., Dover publications, New York,  
 786 1981.

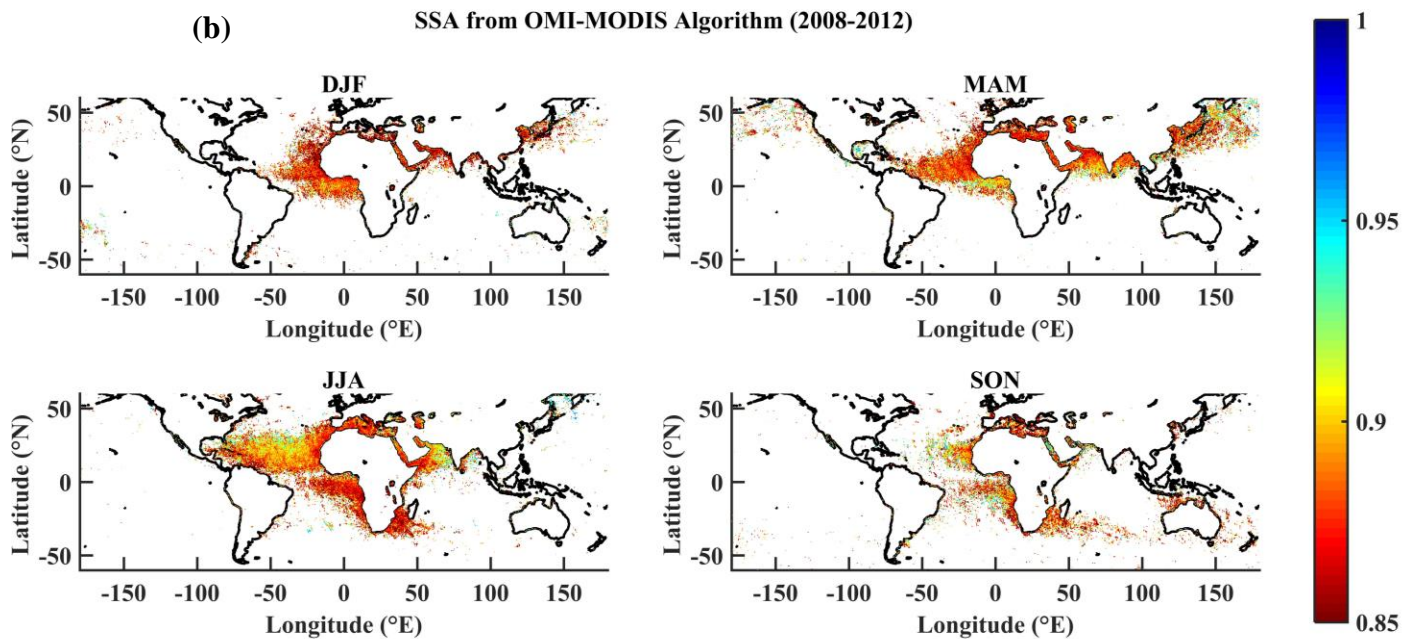
787 Wells, K.C., Martins, J.V., Remer, L.A., Kreidenweis, S.M., and Stephens, G.L.: Critical  
 788 reflectance derived from MODIS: Application for the retrieval of aerosol absorption over  
 789 desert regions, *J. Geophys. Res.*, 117(D3), doi:10.1029/2011JD016891, 2012.

790 Zhu, L., Martins, J.V., and Remer, L.A.: Biomass burning aerosol absorption measurements with  
 791 MODIS using the critical reflectance method, *J. Geophys. Res.*, 116(D7),  
 792 doi:10.1029/2010JD015187, 2011.

793 Zuluaga, M.D., Webster, P.J., and Hoyos, C.D.: Variability of aerosols in the tropical Atlantic  
 794 Ocean relative to African Easterly Waves and their relationship with atmospheric and  
 795 oceanic environments, *J. Geophys. Res.*, 117(D16), doi:10.1029/2011JD017181, 2012.

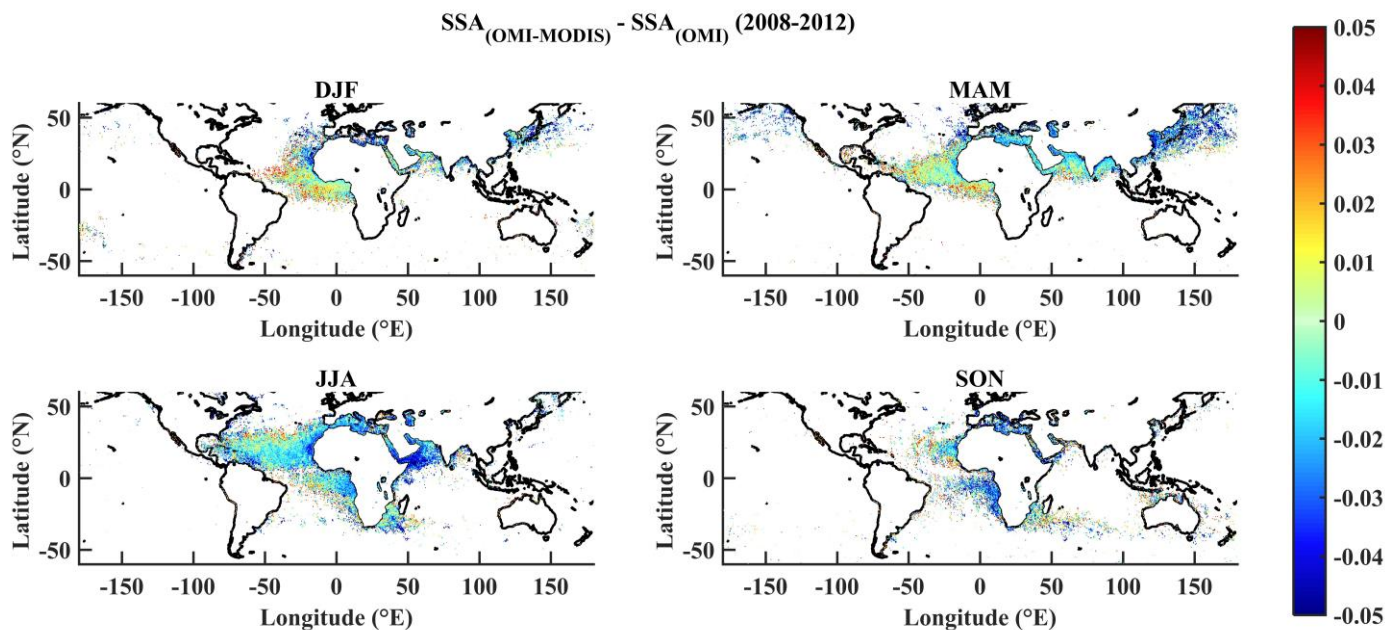


796



797

798 **Figure 1.** Spatial distribution of SSA at 388nm retrieved by a) OMI and b) OMI-MODIS. In the  
 799 present study, points which had the same SSA value at the 5 discrete heights provided by OMI or  
 800 an invalid value at any one height were considered invalid for the OMI-MODIS retrieval since  
 801 interpolation was not possible. This resulted in the reduction of the number of valid points for  
 802 OMI-MODIS when compared to OMI.

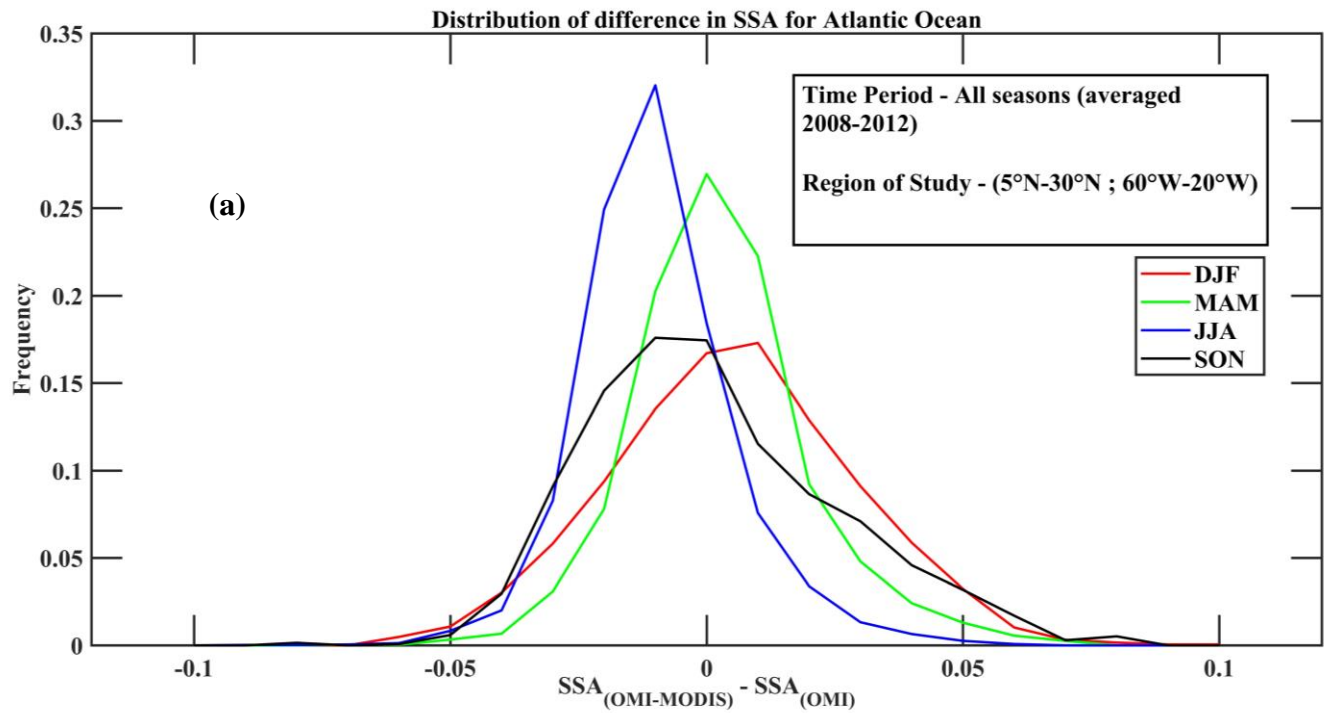


803

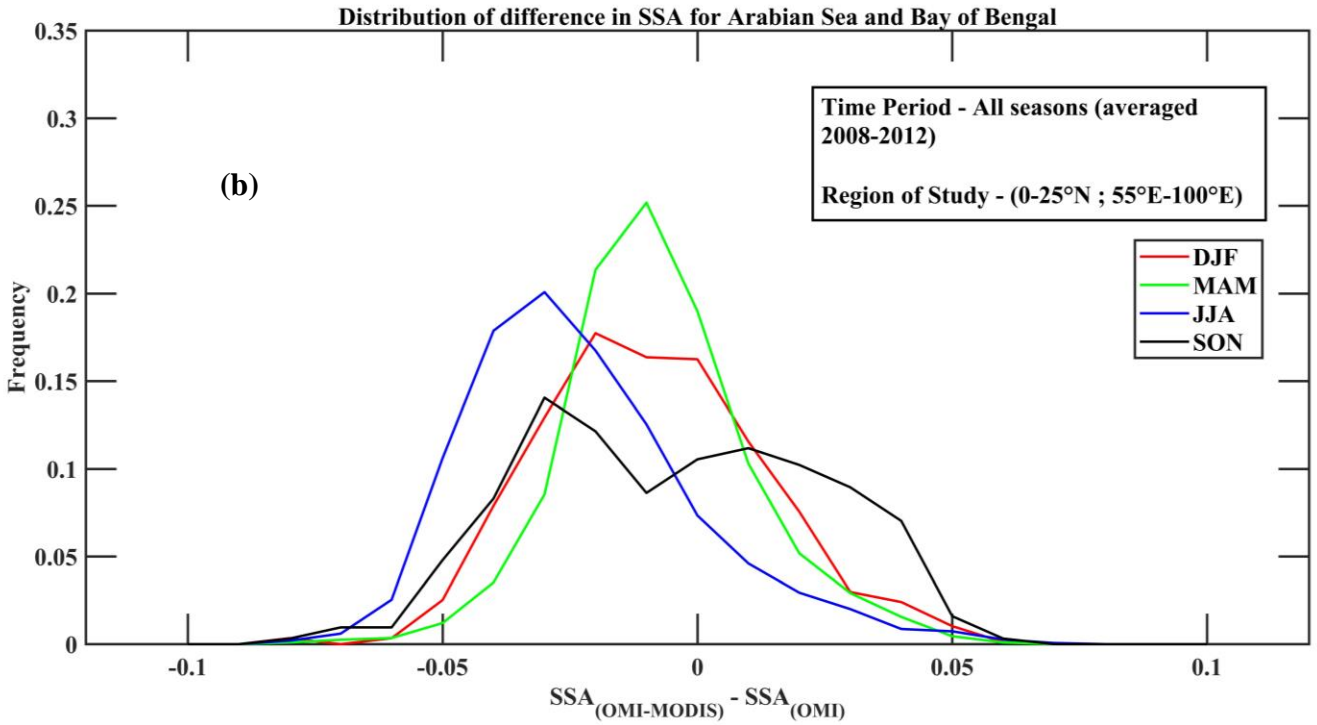
804 **Figure 2.** Spatial distribution of difference in SSA retrieved by OMI-MODIS and SSA retrieved  
805 by OMI, both at 388nm. When the OMI-MODIS SSA value was found invalid, the difference  
806 was also considered to be invalid.

807

808



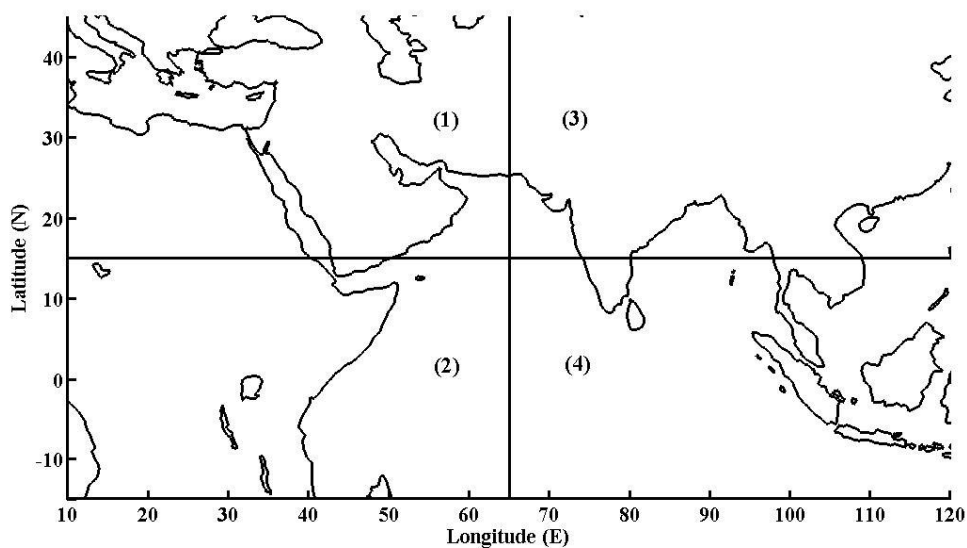
809



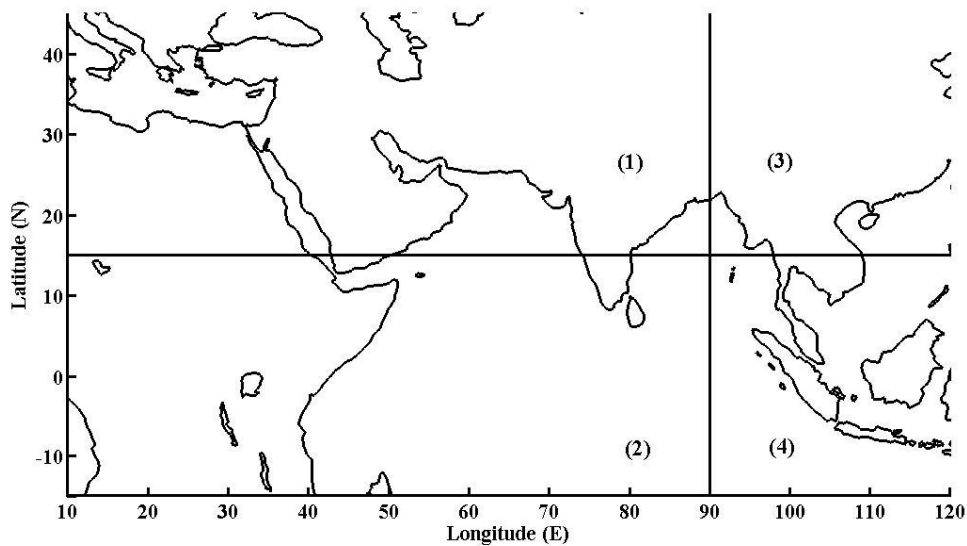
810

811 **Figure 3.** Distribution of difference in SSA for all seasons averaged over 2008-2012 over a)  
 812 Atlantic and b) Arabian Sea and Bay of Bengal. It can be seen that over the Atlantic Ocean, 80%  
 813 of the difference in SSA retrievals was within the  $\pm 0.03$  range. Over the Arabian Sea and Bay of  
 814 Bengal, the retrievals agreed well during the MAM season when the region was influenced by  
 815 dust.

816

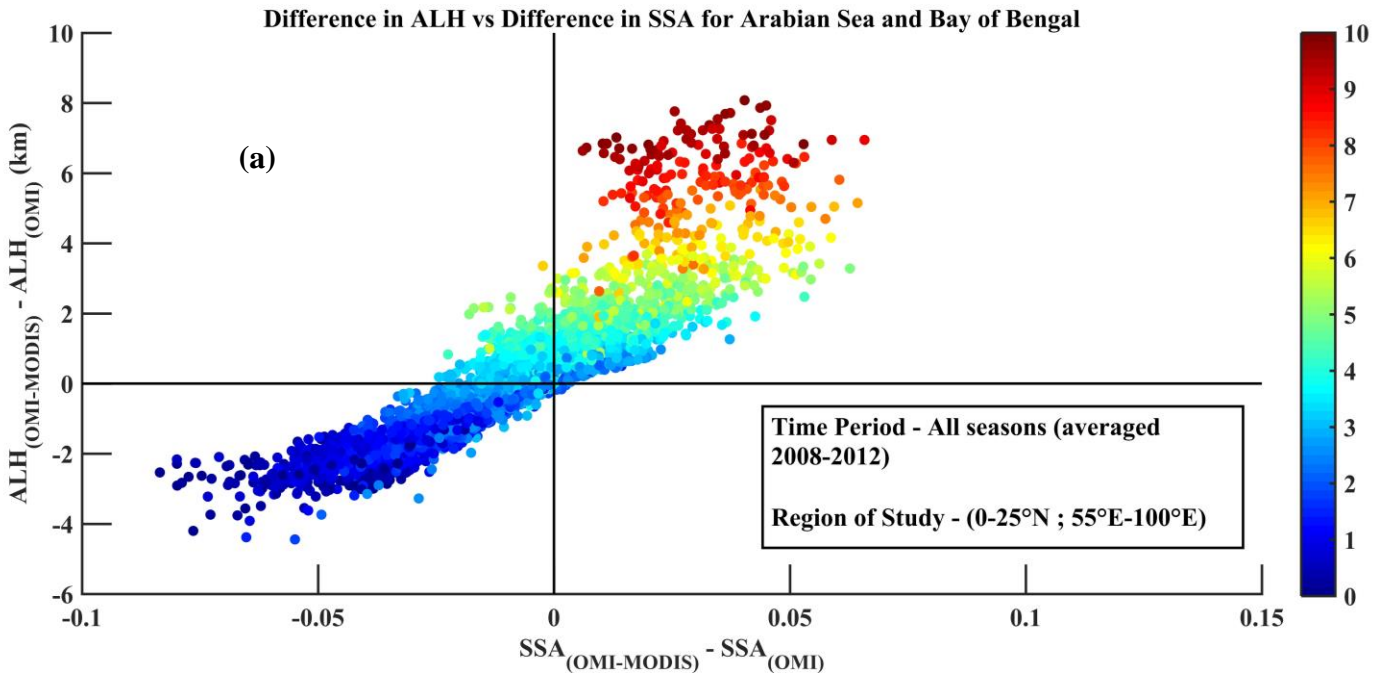


817  
 818 **Figure 4.** Regions representing the various aerosol sources for a point over the Arabian Sea. 1)  
 819 Arabian Peninsula and North Africa, 2) Central Africa, 3) Indian sub-continent and 4) Indian  
 820 Ocean and Southeast Asia.

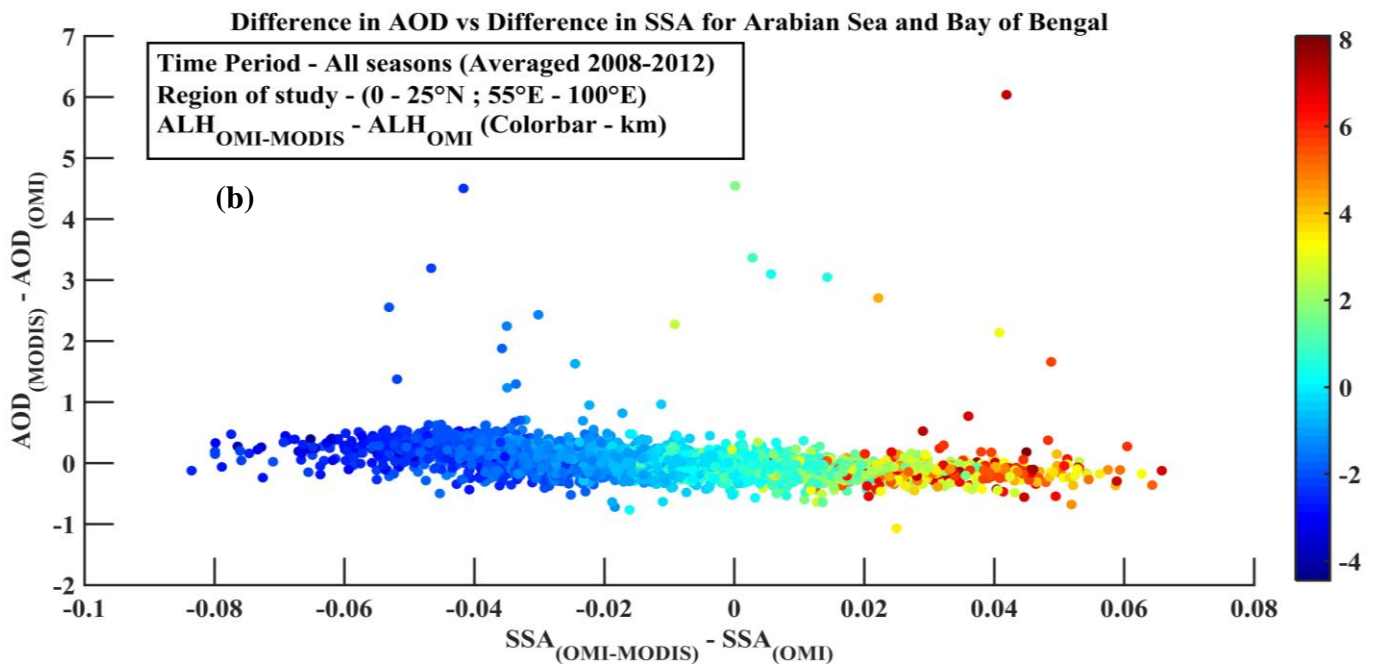


821  
 822 **Figure 5.** Regions representing the various aerosol sources for a point over the Bay of Bengal. 1)  
 823 India/Arabian Peninsula, 2) Indian Ocean, 3) North/Northeast India and East Asia and 4)  
 824 Southeast Asia.

825



826

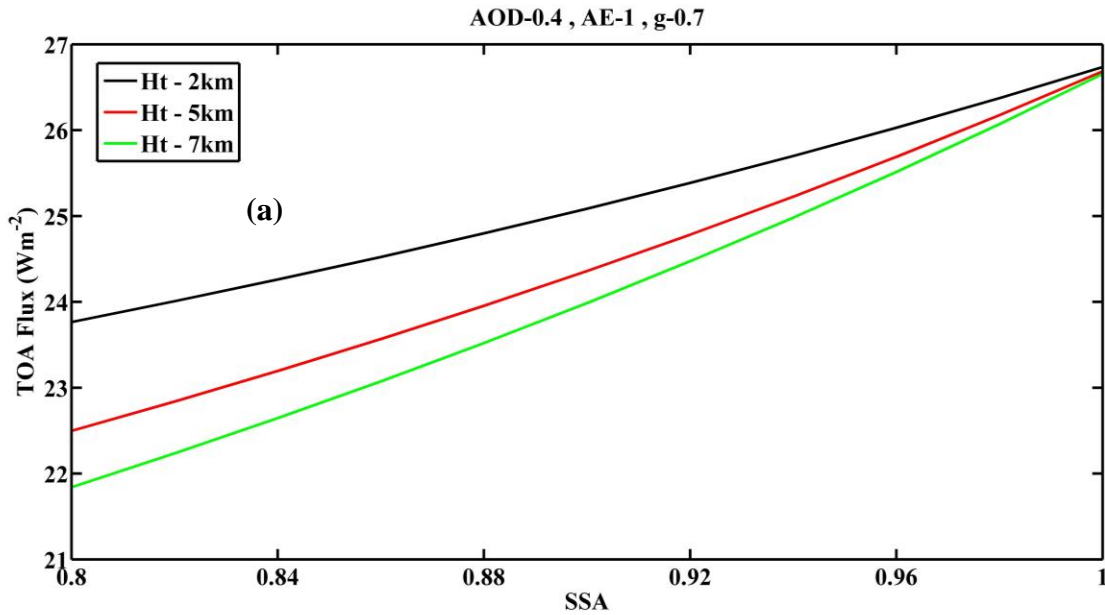


827

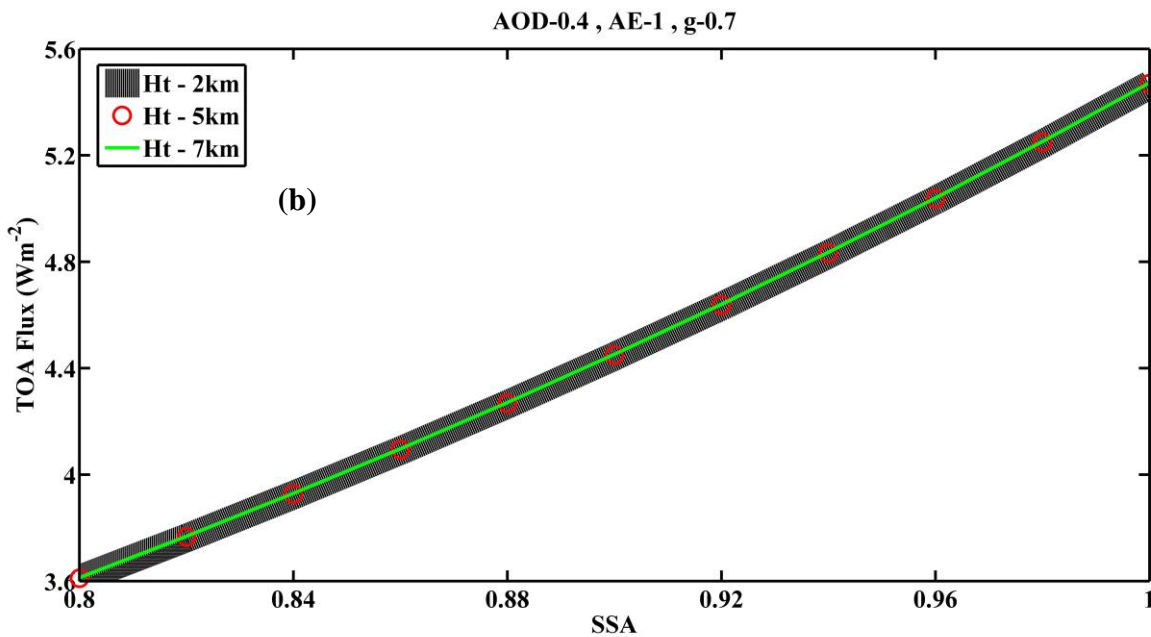
828 **Figure 6.** a) Difference in aerosol layer height (ALH - km) between OMI-MODIS and OMI vs.  
829 difference in SSA over Arabian Sea and Bay of Bengal. The colorbar represents ALH estimated  
830 by OMI-MODIS algorithm (km). At lower height (dark blue circles) estimated by OMI-MODIS



831 OMI overestimated SSA when the ALH was overestimated and vice versa at higher heights  
 832 estimated by OMI-MODIS b) Difference in AOD ( $AOD_{MODIS} - AOD_{OMI}$ ) has been plotted with  
 833 difference in SSA ( $SSA_{OMI-MODIS} - SSA_{OMI}$ ). An inverse relationship was observed. The colorbar  
 834 represents the difference in aerosol layer height (ALH - km) between OMI-MODIS and OMI.  
 835

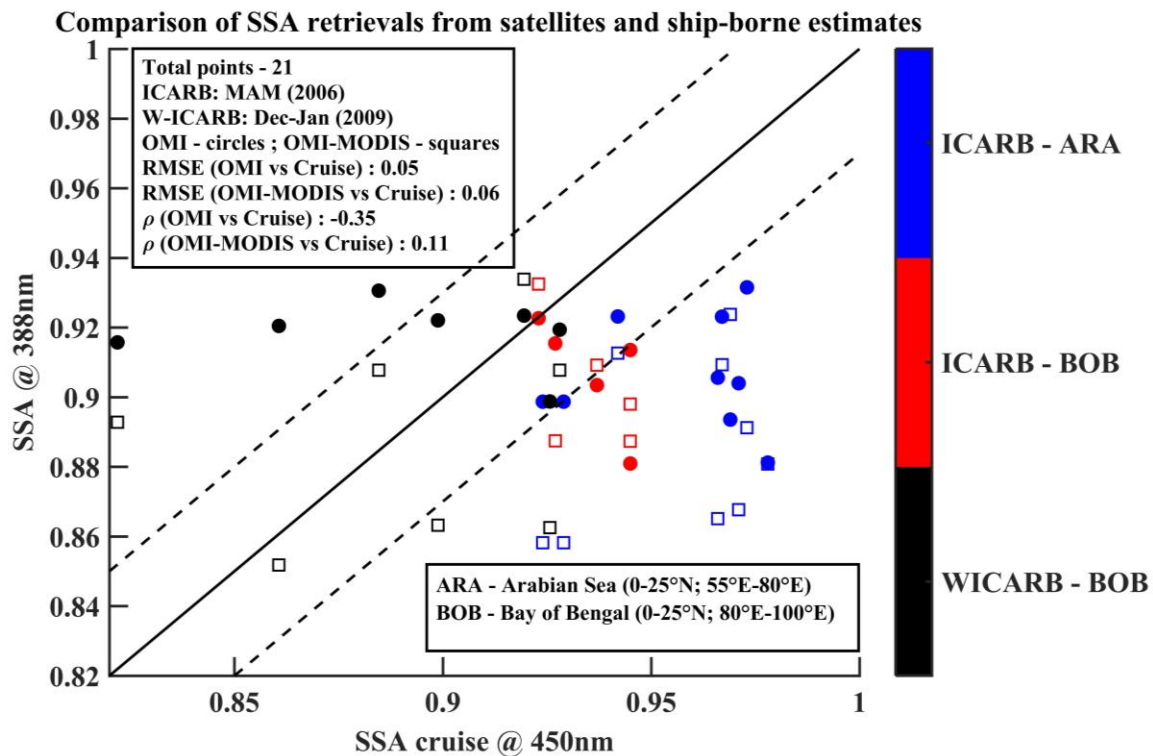


836



837

838 **Figure 7.** TOA flux calculated from SBDART for different SSA and ALH a) with Rayleigh  
 839 scattering and b) without Rayleigh scattering for UV (300-400nm)



840  
 841 **Figure 8.** Comparison of  $SSA_{OMI}$  (circles),  $SSA_{OMI-MODIS}$  (squares) with cruise measurements.  
 842 Each point represents the mean SSA in a  $2^\circ$  box surrounding each cruise location averaged over  
 843 the respective cruise time period. Due to the sparse nature of OMI-MODIS retrieval, the total  
 844 number of points common to both the cruise and satellite estimates is only 21. The solid black  
 845 line is the  $y=x$  line. The dotted lines represent  $\pm 0.03$  range. The colorbar represents the cruise  
 846 name and the region where the measurements are taken. ICARB (Integrated Campaign for  
 847 Aerosols, Gases and Radiation Budget) during March-April-May (MAM) 2006 season; W-  
 848 ICARB (Winter ICARB) during December-January (2008-2009); ARA (Arabian Sea); BOB  
 849 (Bay of Bengal). Discrepancies between the satellite retrievals and cruise measurements were  
 850 seen during the ICARB cruise when elevated aerosols were predominantly present over both the  
 851 regions which might not be detected by the cruise measurements.

<b>References</b>	<b>Method</b>	<b>Technique</b>	<b>Limitation</b>
Herman et al., 1975; King, 1979; Eck et al., 1998; Dubovik and King, 2000; Torres et al., 2005	Ground-based observations	Inverse methods measurements of solar radiances and/or aerosol properties along with radiative transfer calculations	Measurements are spatially and temporally constrained
Dubovik et al., 2002	Global network – Aerosols Robotic Network (AERONET)	Inverse technique using near-real time measured direct and diffuse radiation	Only land-based, low coverage over remote oceanic regions
Kaufman, 1987; Zhu et al., 2011; Wells et al., 2012	Critical surface reflectance - where the net role of aerosol absorption and scattering becomes independent of aerosol optical thickness and is affected only by SSA	Over varying surface reflectance, the radiance difference between clear and hazy skies is measured using satellite images	Limited spatial variability of surface reflectance. Works only for few cases where there are large amount absorbing aerosols present

Kaufman et al., 2002b	Retrieve SSA in visible wavelengths	Sun-glint is used as a bright background to differentiate role of scattering from aerosol absorption	Only limited scenarios present and does not work on land when absorbing aerosols are present (Torres et al., 2005).
Diner et al., 1998; Remer et al., 2005	Multi Angle Imaging Spectroradiometer (MISR) and Moderate Resolution Imaging Spectroradiometer (MODIS)	Retrieves AOD and SSA in the visible and infrared region of solar spectrum	Surface reflectance influences the retrievals
Herman et al., 1997; Torres et al., 1998	Total Ozone Mapping Spectrometer (TOMS)	Aerosol index parameter is highly sensitive to the Rayleigh scattering thus acting as a bright background in the UV regime	Large pixel size prone to cloud contamination
Torres et al., 2002	Ozone Monitoring Instrument (OMI)	Similar technique as TOMS. Pre-defined aerosol models used.	Sensitive to aerosol layer height and still prone to cloud contamination

852

853 **Table 1.** Ground-based and Satellite-based indirect methods to retrieve SSA

854

855

Seasons \ Regions		1	2	3	4
DJF	500m	<b>57%</b>	0%	38%	5%
	1500m	<b>62%</b>	10%	19%	9%
	2500m	<b>81%</b>	14%	0%	5%
MAM	500m	19%	<b>43%</b>	19%	19%
	1500m	29%	<b>29%</b>	23%	19%
	2500m	<b>57%</b>	14%	24%	5%
JJA	500m	0%	24%	0%	<b>76%</b>
	1500m	19%	<b>67%</b>	0%	14%
	2500m	<b>62%</b>	33%	5%	0%
SON	500m	5%	24%	<b>47%</b>	24%
	1500m	14%	19%	<b>48%</b>	19%
	2500m	<b>38%</b>	10%	19%	33%

856

857 **Table 2.** Influence of various aerosol sources over Arabian Sea given as percentage of  
 858 trajectories originating from each source respectively. The maximum influence is given in black  
 859 bold. The different source regions are explained in text and Fig. 4.

Seasons \ Regions		1	2	3	4
		DJF	500m	<b>72%</b>	0%
	1500m	<b>48%</b>	14%	10%	28%
	2500m	29%	33%	0%	<b>38%</b>
MAM	500m	19%	<b>48%</b>	0%	33%
	1500m	<b>57%</b>	29%	20%	14%
	2500m	<b>71%</b>	24%	0%	5%
JJA	500m	0%	<b>100%</b>	0%	0%
	1500m	5%	<b>95%</b>	0%	0%
	2500m	14%	<b>81%</b>	0%	5%
SON	500m	5%	<b>52%</b>	33%	10%
	1500m	5%	<b>43%</b>	<b>43%</b>	9%
	2500m	5%	<b>33%</b>	29%	<b>33%</b>

861

862 **Table 3.** Influence of various aerosol sources over Bay of Bengal given as percentage of  
863 trajectories originating from each source respectively. The maximum influence is given in black  
864 bold. The different source regions are explained in text and Fig. 5.

865